www.sciencemag.org/cgi/content/full/333/6042/596/DC1

Supporting Online Material for

Independently Evolved Virulence Effectors Converge onto Hubs in a Plant Immune System Network

M. Shahid Mukhtar, Anne-Ruxandra Carvunis, Matija Dreze, Petra Epple, Jens Steinbrenner, Jonathan Moore, Murat Tasan, Mary Galli, Tong Hao, Marc T. Nishimura, Samuel J. Pevzner, Susan E. Donovan, Lila Ghamsari, Balaji Santhanam, Viviana Romero, Matthew M. Poulin, Fana Gebreab, Bryan J. Gutierrez, Stanley Tam, Dario Monachello, Mike Boxem, Christopher J. Harbort, Nathan McDonald, Lantian Gai, Huaming Chen, Yijian He, European Union Effectoromics Consortium, Jean Vandenhaute, Frederick P. Roth, David E. Hill, Joseph R. Ecker, Marc Vidal,* Jim Beynon,* Pascal Braun,* Jeffery L. Dangl*

*To whom correspondence should be addressed. E-mail: dangl@email.unc.edu (J.L.D.); pascal_braun@dfci.harvard.edu (P.B.); jim.beynon@warwick.ac.uk (J.B.); marc_vidal@dfci.harvard.edu (M.V.)

Published 29 July 2011, *Science* **333**, 596 (2011)
DOI: 10.1126/science.1203659

This PDF file includes

Materials and Methods
SOM Text
Figs. S1 to S18
Tables S3 to S5
Glossary
References

Other Supporting Online Material for this manuscript includes the following Excel tables: (available at www.sciencemag.org/cgi/content/full/333/6042/596/DC1)

Table S1. Immune-related pathogen and plant proteins used to construct Plan Pathogen Immune Network (PPIN-1).
Table S2. Plan Pathogen Immune Network (PPIN-1).
Table S6. Subdivision of PPIN-1 into 10 nonoverlapping groups of proteins.
Table S7. Enrichment of groups of PPIN-a in differentially expressed (DE) genes that were determined form defense-related experiments.
Table S8. List of significant targets present in AI-1_{MAIN}

Table S9. Lists of the combinatorial modules indicated in Fig. 3, B and C.
Table S10. Infection results for validation of targets shown in Fig. 4.

Author contributions:

M.S.M.: initiation of project, lead for experimental design and Y2H analyses, data analyses, and writing the manuscript.

A.-R.C.: lead for bioinformatics analyses, database design, and writing the manuscript.

M.D.: lead for Y2H analyses, experimental quality control, data analysis, and writing the manuscript.

P.E.: validation of 18 common pathogen effector targets, data for Fig. 4, A and B, and table S10, and writing the manuscript.

J.S.: network data analysis.

J.M.: evolutionary analyses of pathogen targets and mRNA expression analyses.

M.T.: BS: support for statistical analyses.

M.G.: quality control of Y2H data.

T.H.: database design and analysis of all IST sequencing traces.

M.T.N.: provided experimentally validated type III effector clones.

S.J.P.: statistical analysis of connectivity shown in Fig. 2B.

S.E.D.: participation in Y2H screening of *H. arabidopsidis* ORFs and making groups of *H. arabidopsidis* ORFs and network data analysis.

L.G.: Y2H screening of *H. arabidopsidis* ORFs and verification of interactions.

V.R., M.M.P., F.G., B.J.G., S.T., D.M., M.B.: Y2H pipeline.

C.J.H.: validation of Y2H *P. syringae* data and assistance with Fig. 4.

N.M.: genotyped all validation mutants for Fig. 4 A and B.

L.G., H.C.: web-based visualization of PPIN-1.

Y.H.: bacterial infection assays for fig. S12B.

J.V.: discussion of Y2H analyses and experimental quality control data.

F.P.R.: discussion, oversight of statistical analyses.

D.E.H.: oversight of CCSB operations.

J.R.E.: discussion, analyses, provision of *A. thaliana* ORFs.

M.V.: conception and planning of project, discussion and oversight of analyses.

J.B.: planning of project, organization of *Hpa* candidate effector clones.

P.B.: conception and planning of project, oversight of Y2H and quality control and statistical analyses, and writing the manuscript.

J.L.D.: conception and planning of project, oversight of biological validation experiments and analyses, and writing the manuscript.

Materials and Methods:

Selection and cloning of ORFs encoding Arabidopsis immune proteins.

1- Cytoplasmic domains of leucine-rich repeat (LRR)-containing receptor like kinases (RLKs), a subclass of pattern-recognition receptors (PRRs). The Arabidopsis genome encodes 610 predicted PRRs including 216 RLKs. They consist of an extracellular LRR domain, a transmembrane domain and a cytoplasmic serine/threonine kinase domain (*36*). Several LRR domains have been shown to directly bind a ligand, while the kinase domain is vital for downstream signaling. Only a limited number of RLKs have been ascribed any function, and only a few of these are reported to act as immune receptors (*3, 19, 37, 38*). Transcriptome data suggests that the overwhelming majority of LRR kinase genes are down-regulated by pathogen effector delivery, compared to expression following PRR stimulation (*19, 37, 39*). We included almost a family-wide collection (179) of cytoplasmic domains from LRR-RLKs (**fig. S1**, **table S1**).

2- N-terminal domains of NB-LRR proteins. Nucleotide binding site leucine-rich repeats (NB-LRR) proteins are closely related to animal NLR immune receptors and form the major R protein class in Arabidopsis with ~150 members (*6, 7, 40*). The NB-LRR family of proteins is further subdivided based on the presence of an N-terminal Toll/Interleukin-1 Receptor (TIR) or coiled-coil (CC) motif. NB-LRR proteins likely exist in intra- and intermolecular folded conformers before activation. N-terminal domains of NB-LRRs are thought to be negatively regulated by the LRR domain. Effector and/or effector-target binding is thought to relieve this intramolecular repression and allow nucleotide binding and signal competence. Moreover, N-terminal domains of NB-LRRs can be involved in association with either cellular targets of effector action or with recruitment of downstream signaling components (*6, 7, 40*). Thus, we cloned sequences encoding N-terminal domains of NB-LRRs from Col-0. In some cases, we also included full-length or other than N-terminal domains of an NB-LRR. In total, we included 144 clones corresponding to 136 loci (**fig. S1**, **table S1**). These included N-termini from the well studied RPM1, RPS2, and RPS5 proteins.

3- Effector proteins from the bacterial pathogen *Pseudomonas syringae (Psy)* and the oomycete pathogen *Hyaloperonospora arabidopsidis (Hpa)*. These effector proteins are critical virulence determinants that target host proteins. While Gram-negative bacteria use the type III secretion system to deliver type-III effectors, little is known about the mechanism(s) of delivery of oomycete effectors into host cells (*41*). Oomycete cytoplasmic effectors are modular proteins that carry N-terminal signal peptides followed by conserved motifs, notably the RXLR and LXLFLAK motifs (*42*). We cloned 101 coding sequences for translocation confirmed *Psy* type III effectors from 16 different bacterial strains (*8*). Included among these were three effectors (AvrRpm1, AvrB, AvrPphB-mature fragment, and AvrRpt2-mature fragment) that are known to interact with Arabidopsis targets in a manner that leads to activation of either the RPM1, RPS2, or RPS5 NB-LRR from Col-0. Note that these are all indirect activation events and that two, activation of RPS5 and RPS2, require cleavage of the relevant host target by the protease effectors. Thus, we would not expect to recover these in our screen,

consistent with previous efforts. We did recover the interaction of AvrB with RIN4. Moreover, we also cloned coding sequences for 131 *Hpa* RXLR/LXLFLAK candidate effector proteins from 17 different isolates (Ahco2, Aswa1, Bico1, Bico5, Cala2, Cand5, Emco5, Emoy2, Emwa1, Hiks1, Hind2, Hind4, Maks9, Noks1, Waco5, Waco9, Wela3). The *Hpa* candidate effectors were cloned from spore DNA from the predicted signal peptide cleavage site (or otherwise stated in **table S1**) to the predicted stop codon (*9*). For network analyses, we collapsed alleles and domain subclones corresponding to the same effector protein and thus generated 58 and 99 effector groups for *Psy* and *Hpa*, respectively (**fig. S1ig. 1A**, **table S1**).

4- Defense proteins. We included 91 clones corresponding to 77 known signaling components and previously described host targets of pathogen effectors. Collectively, we refer to this sub-class as “defense proteins” (**fig. S1**, **table S1**).

5- Cloning of ORFs encoding immune proteins. Total RNA was isolated from Arabidopsis (ecotype Columbia-0, unless noted) leaves using Trizol reagent (Invitrogen, Carlsbad, CA). First-strand cDNA was synthesized using RETRO script reverse transcriptase (Ambion). The cDNA products were amplified using AccuPrime *Pfx* DNA Polymerase (Invitrogen). For cloning of *Psy* type III effector and *Hpa* RxLR effector encoding genes, DNA was isolated from the appropriate strain/isolate and used for PCR. The PCR primers contained the *att*B1 and *att*B2 or CACC sequences for cloning PCR products into pDONR vectors or pENTR-D-TOPO series of vectors, respectively, by Gateway BP recombinational or TOPO cloning (Invitrogen). We obtained clones for RLK intracellular domains consisting of sequences encoding the juxtamembrane region, catalytic kinase domain and carboxy terminal region of each LRR RLK in the vector pDONR/zeo from Invitrogen. Stock numbers of the RLKs clones that were obtained from ABRC are given in **table S1**. Domains of NB-LRR proteins were predicted by TAIR. DNA sequences upstream of NB-ARC encoding region were considered N-terminal region (for both CC and TIR) and cloned.

Yeast Two-Hybrid (**Y2H) Screening.**

First, Gateway entry clones were transferred into pDEST-DB and pDEST-AD-*CYH2* yeast two-hybrid destination vectors to generate Gal4 DNA binding domain (DB)-X hybrid proteins and Gal4 activation domain (AD)-Y hybrid proteins, respectively. The detailed procedure for Y2H screening is described in Dreze *et al.* (*11*). This strategy was applied to identify interactions in a systematic manner between pathogen effectors, NB-LRRs, RLKs, defense proteins and proteins in AtORFeome2.0. Briefly, the yeast strains Y8930 (*MAT*α) and Y8800 (*MAT***a**) were transformed with individual plasmids encoding DB-X and AD-Y constructs, respectively, resulting in DB-X and AD-Y yeast strains. Prior to Y2H selections, each DB-X yeast strain was examined for auto-activation of the *GAL1-HIS3* reporter gene in the absence of any AD-Y. All yeast strains showing elevated expression of the *GAL1-HIS3* reporter gene were removed from the collection while non auto-activating DB-X strains were used for Y2H screen. In a first step, each DB-X yeast strain was tested for possible interaction against mini-libraries of 192 AD-Y yeast strains. This first step was completed twice to increase sampling depth. The phenotype of the resulting primary positives was then tested again in a second step

and only those whose phenotype could be confirmed (secondary positives) were retained for identification of DB-X and AD-Y pairs by end-read sequencing of PCR products amplified directly from yeast cells. In a third and final step, the phenotype of these candidate Y2H interactions was then verified in a pairwise manner (1 DB-X vs 1 AD-Y) four times, by four different experimenters. In addition, at each of the three processing steps, we tested the phenotype of DB-X yeast strains for possible spontaneous DB-X auto-activation events and removed them when detected. We also tested the phenotype of each AD-Y yeast strain for infrequent yet possible AD-Y auto-activation and removed them when observed. In sum, only pairs whose phenotype could be verified at least three times out of four and that did not show any auto-activation were considered Y2H interactions. Since the identification of candidate Y2H interactions is done based on end-read sequences, it is difficult to differentiate nearly identical sequences, *i.e.* alleles, hence to assign interactors to the correct allele. To circumvent this problem, in the third step of the Y2H strategy we systematically verified, within group of alleles, each interactor against each allele.

The extremely low number of available literature-curated pathogen effector-Arabidopsis interactions (*16*) precluded the construction of a reliable positive reference set for use in estimating the pathogen-host-specific interaction quality. Previous interactome datasets of several species (*13, 15, 43-45*) were estimated to have similarly high precision (fraction of true interactions), supporting the notion that the reliability of this screen technology is species independent. For full details on the precision computation, please refer to the accompanying paper (*11*).

Statistical analyses.

Probabilities for the following overlaps between pairs of datasets were estimated using a hypergeometric test:

- Immune interactors and GO-immune annotated proteins from AtORFeome2.0
- GO-immune proteins and effector targets
- Hormone-related proteins and effector targets
- $Hubs_{50}$ and effector targets (all, significant and common)
- Significant targets and common targets
- Indirect connections between effectors and receptors (NB-LRRs and RLKs)
- Effector targets with orthologs in angiosperms only and more broadly conserved effector targets.
- Proteins encoded by differentially expressed (DE) defense genes and proteins in PPIN-1 (all and subgroups)

Contingency tables for these tests are presented in **tables S4** and **S7.** GO-term (*46*) enrichments for the effector target proteins were estimated using the FuncAssociate R library (*47*), with a false discovery rate cutoff of 20%, using proteins in $AI\text{-}1_{MAIN}$ as a reference set to control for ORF collection and Y2H potential biases. Only targets that were not in the original immune protein sets were considered for this analysis. The results describing more than 10% of these effector targets and representing an enrichment of more than 1.25 with an adjusted p-value inferior to 0.2 are presented in **table S5**.

Identification of ortholog clusters.

We identified ortholog clusters between proteins in Arabidopsis and other species pairwise using the InParanoid resource (*48*). We chose the following species to provide a broad taxonomic sample between Arabidopsis and more distant taxa: *Populus trichocarpa, Oryza sativa, Sorghum bicolor, Physcomitrella patens, Cyanidioschyzon merolae, Ostreococcus tauri, Chlamydomonas reinhardtii, Thalassiosira pseudonana, Neurospora crassa, Saccharomyces cerevisiae, Caenorhabditis elegans, Drosophila melanogaster, Homo sapiens, Escherichia coli* K12. For each Arabidopsis gene we identified its most distant ortholog(s), and its "phylogenetic footprint" according to the above taxonomic sampling scheme. To control for homoplasy, we identified instances of phylogenetic footprints being sparsely populated but over-represented in our data, in other words, cases where an Arabidopsis gene apparently had a very distant ortholog but no or very few orthologs in other intermediate species, and where such footprints occurred at least 1.5 times more frequently than expected given the overall proportions of orthologs we found in each species. In these cases, we removed the most distant ortholog from the footprint. The main effect of this filtering was that a number of genes with apparent orthologs in animal taxa, but none in other more closely related taxa, were reassigned to being Arabidopsis-specific genes.

Having identified a definitive list of "most distant ortholog(s)" for each Arabidopsis gene, where we also had evidence of orthologs being present in more closely related taxa, we classified each Arabidopsis gene as being 'angiosperm-specific' (where no ortholog was found, or where the most distant ortholog was found in *P. trichocarpa, O. sativa* or *S. bicolor*), or "more broadly conserved" (where orthologs were found in angiosperms and also in more distant taxa). Angiosperm-specific proteins are over-represented among the effector targets that are present in AtORFeome2.0, in comparison with all of AtORFeome2.0 (hypergeometric $P = 0.0007$; **table S4**).

Differentially Expressed (DE) genes.

Results were mined from nine previously published studies of transcriptional responses of Arabidopsis to pathogen or other immune system related perturbations (**table S7**, *37, 49-56)*. Priority was given to well-referenced studies, employing the Affymetrix ATH1 GeneChip array, encompassing overall a broad range of different perturbations. Lists of probes showing significant up- or down-regulation in each experimental condition were compiled, using criteria for significance employed in the respective original study. Probe lists were mapped to the TAIR7 genome, and filtered to only include probes corresponding to unique proteins in the AI-1_{MAIN} network with a TAIR7 gene model. Subgroups of proteins in PPIN-1 were tested for enrichment or depletion of differentially regulated genes in individual experiments, and for the number of times genes were differentially regulated across all experiments, in comparison to proteins in AI-1_{MAIN}, using a hypergeometric test (**table S7**).

d_N/d_S measurement.

Gene models of orthologs between Arabidopsis and Papaya genes were identified by aligning coding sequences using BLAST (*57*) and selecting reciprocal best hits. In order to stringently assess whether immune interactors are evolving more rapidly under pathogen pressure, potentially faster evolving paralogous genes were excluded

from subsequent analyses, and only one-to-one orthologs were processed further. Coding sequences of orthologous gene pairs were aligned in protein space using a custom workflow employing Clustal (*58*). The ratio of non-synonymous to synonymous mutations per site in coding sequences (d_N/d_S) was estimated for each aligned gene pair using the maximum likelihood codon substitution model method of (*59*) in the PAML package codeml program (*60*), allowing d_N/d_S to vary between branches, and estimating kappa and omega parameters from data. Values of d_S were found saturated in a small fraction of orthologs, so subsequent analyses were carried out both with and without the 15% of ortholog pairs for which $d_S>5$. Removal of these d_S-saturated orthologs did not qualitatively affect our results, but increased the observed significance levels. Significant differences between distribution of d_N/d_S within each subgroup of genes in the pathogen network, and distribution of d_N/d_S among all genes in AI-1_{MAIN}, were identified using a Kolmogorov-Smirnov test of significance.

Poplar orthologs were also tried, as a basis for d_N/d_S calculations, and results were found positively correlated with those calculated from Papaya orthologs (r=0.84 for immune network genes), but were found to be d_S–saturated in many more cases. Papaya was ultimately used as its genome is fully sequenced, it shares membership of the Brassicales with Arabidopsis so d_N/d_S represents more recent evolutionary events, and the two are sufficiently diverged for d_N/d_S to be estimated, but not so distant that d_S is saturated, in most cases.

Network analyses.

All calculations and simulations regarding network properties were performed using the R implementation of igraph (*61*). All network representations were drawn using Cytoscape (*62*).

1- Computational simulations of random targeting of Arabidopsis proteins by effector targets: convergence of effectors onto a limited set of targets.

To estimate how many Arabidopsis targets of pathogen effectors would be expected by chance alone, we performed 1,000 computational randomizations as follows. We considered the union of all PPIN-1 and AI-1 Arabidopsis proteins as “Y2H-amenable”. We counted the number of Arabidopsis proteins each effector connected to in PPIN-1 then selected the same number of proteins at random from the set of Y2H amenable proteins. We repeated this process for all effector proteins in PPIN-1, then counted: (i) the total number of Arabidopsis proteins selected by this process (total number of “random targets”, **Fig. 2A**; left panel); and (ii) the proportion of these random targets found connected by effectors from the two pathogen species by chance (proportion of random shared targets, **Fig. 2A**; right panel). A typical result of these simulations is shown in **fig. S7A** and **fig. S8** in comparison with the observed data in PPIN-1.

2- Computational simulations of random targeting of Arabidopsis proteins by effector targets: connectivity between targets.

To estimate how many direct interactions between effector targets would be expected by chance alone, we considered that the number of effector targets remains constant (as opposed to **Fig. 2A**), but that they are randomly distributed in AI-1_{MAIN}. We

performed 15,000 network randomizations based on AI-1_{MAIN} where the names of proteins were randomly shuffled while keeping the network structure intact, and counted the number of direct interactions between targets in the randomized network (total number of direct interactions between targets, **Fig. 2B**).

3- Computational simulations of random targeting of Arabidopsis proteins by effector targets: identification of significant targets.

We define "significant targets" as the set of Arabidopsis proteins that establish more interactions with effector proteins in PPIN-1 than what would be expected given their degree in AI-1_{MAIN} under the assumption that effector-target interactions are a consequence of the propensity of a protein to bind other proteins. This analysis was restricted to the 137 effector targets (out of 165 total) present in AI-1_{MAIN}. We counted the number of interactions between effectors and targets in PPIN-1, then selected that number of AI-1_{MAIN} proteins at random with replacement, with a probability proportional to their degree in AI-1_{MAIN}. This process was repeated 1,000 times. As a result, we were able to compare the number of interactions that each of the 137 targets has with effectors in PPIN-1 with a distribution of 1,000 expected numbers from these simulations. When less than 5% of the simulations generated a number equal to or greater than the experimentally determined number, the target was considered a significant target. This process identified 51 significant targets, including five $hubs_{50}$ (**Fig. 2D; table S8**). Interestingly, ANAC089 (AT5G22290) is only connected to one effector in PPIN-1 despite having a degree of 222 in AI-$1_{MAIN,}$ which makes it appear significantly avoided by effectors in our experiment.

Plant materials and growth conditions.

We used *Arabidopsis thaliana* Columbia (Col-0) unless mentioned otherwise. Insertion mutants are listed in **table S10**. Three additional T-DNA knock-out lines for At3g47620 (AtTCP14), *attcp14-4* (GK-861-G08), *attcp14*-5 (GK-611-C04) and *attcp14-6* (SAIL_1145_H03)) were obtained from the European Arabidopsis Stock Center (NASC;(*29, 63*). *attcp14-1*, *attcp14-2* and *attcp14*-3 are previously described (*64*). *cul3a* (SALK_050756) and *csn5a-2* (SALK_027705) *cul3a* (SALK_050756) double mutant were provided by Xing-Wang Deng (*32, 65*) and the *pfd6-1* (CS16396) mutant was a gift from Chris Somerville's lab (*66*). Plants were grown under short day conditions (9 hrs light, 21°C; 15 hrs dark, 18°C except for *attcp14* mutants, which were grown under a 10 hrs light, 14 hrs dark cycle).

***Hyaloperonospora arabidopsidis (Hpa)* isolates, infections, and growth assays.**

Hyaloperonospora arabidopsidis (*Hpa*) isolates Emwa1, Emoy2, Emco5, Noco2, or Noks1 were propagated on the susceptible Arabidopsis ecotypes Ws, Oy-1 and Col-0, respectively (*67, 68*). Twelve day old seedlings were infected with conidiospores suspended in water at the appropriate concentration (30,000 spores/ml, *Hpa* Emwa1; 40,000 spores/ml, *Hpa* Emoy2; 30,000 spores/ml *Hpa* Noco2; 50,000 spores/ml *Hpa* Emco5) and three-week old adult plants were infected with 10,000 spores/ml, *Hpa* Noks1 (*69*). Plants were kept covered with a lid to increase humidity and grown at 20°C with a 9 hrs light period.

Sporangiophores were counted on cotyledons at 4 or 5 days post-infection (dpi) as described (*70*). The number of sporangiophores per cotyledon was determined and percentages were calculated as described (*70*). For Noks1, the number of spores per fresh weight of 10 plants was calculated at 6 dpi (6 replicates per experiment).

Bacterial infection experiments.

The flg22-dependent MTI experiment was performed as reported in (*19*). Briefly, four-week old plants were injected with 1μM flg22 24hrs prior to infection with *P. syringae* DC3000 (-1 day). flg22-injected leaves were then infiltrated with a concentration of ~$1x10^5$ colony forming units (cfu)/ml (OD_{600} = 0.0002) of *Psy via* a needle-less syringe. Plants were covered for ~24hrs post-inoculation with a lid. Leaf discs were cored from the infiltrated area at the day of infiltration (0 dpi) and 3 dpi, ground in 10 mM $MgCl_2$, and serially diluted to measure bacterial numbers. For each sample, four leaf discs were pooled six times per data point (24 leaf discs total).

P. syringae DC3000(*avrRpt2*) growth assays were performed as previously described (*70*) with modifications. Briefly, bacteria were resuspended in 10 mM $MgCl_2$ to ~$1x10^5$ cfu/ml and syringe infiltrated into leaves of ~four-week old wild type and mutant plants. Leaf discs were cored from the infiltrated area on the day of infiltration (0 dpi) and 3 dpi, placed in 10 mM $MgCl_2$ containing 0.02% v/v Silwet L-77, shaken for 1 hr at 28°C (250 rpm), and serially diluted to count colony forming units. For each sample, four leaf discs were pooled four times per data point (16 leaf discs total).

Detailed rationale for validation of Prefoldin 6 (PFD6; At1g29990).

PFD6 forms heterohexameric complexes and belongs to the chaperone family of proteins required in protein folding complexes and found in the cytosol of archaea and eukaryotes but absent from bacteria (*71*)**.** Prefoldin works in combination with other molecular chaperones to correctly fold nascent proteins. PFD6 interacts with EDS1, an essential component of both MTI and some ETI pathways that also plays a key role in salicylic acid dependent plant defense signaling pathways (*72*). Both HopAO1 and AvrPto, which interact with PFD6, can suppress MTI (*1, 3, 16, 38*). Prefoldin 6 is required for normal microtubule dynamics and organization in Arabidopsis (*66*). The *pfd6-1* mutant exhibits a range of microtubule defects, including hypersensitivity to oryzalin, defects in cell division, cortical array organization, and microtubule dynamicity. Oryzalin is a dinitroaniline herbicide that sequesters tubulin dimers (*66*). Moreover, flg22-dependent endocytosis of the FLS2 LRR-K PRR was inhibited by oryzalin (*33*).

Real time RT-PCR and Western blotting.

Total RNA was isolated using Trizol reagent (Invitrogen) from 100 mg fresh tissue that was treated with 1μM flg22 for 45 minutes via syringe-infiltration. DNase treatment was performed using the DNA-*free* reagent (Ambion) for 20 min at 37ºC, according to the manufacturer's instructions. Three micrograms of RNA were used as starting template material for first strand cDNA synthesis using RETROscript reverse transcriptase (Ambion). Real time PCR was performed using the primers corresponding to MTI-responsive markers as indicated in **fig. S13**. For detection of PR-1 accumulation, total protein extracts were prepared from leaf tissue infected with the *Hpa* isolate Emco5 for 2 days as described above or injected with the virulent bacterial strain *P. syringae*

DC3000at a concentration of 10^5 cfu/ml via a needle-less syringe for 24hrs. Western blots were performed by using standard methods (*73*). Anti-PR1 serum (gift of Dr. Robert A. Dietrich, Syngenta, Research Triangle Park, NC) was used at a dilution of 1:10,000. Anti-CSN5 (Z04911; BMLPW8365- 0100) detects both CSN5a and CSN5b subunits, and was used according to the manufacturer' instructions (BIOMOL).

Local interactome networks of the five most significantly targeted hub_{50} proteins.

To facilitate hypothesis development the following section describes the local interactome network of the five significantly targeted hubs and possible functional connections related to infection and immune system function. Because this analysis includes information that is not systematically available for all proteins in AI-1_{MAIN}, no p-values can be provided.

AtTCP14 (AT3G47620). The transcription factor AtTCP14, a hub_{50} in AI-1_{MAIN}, is targeted by both pathogens collectively 29 times (P <0.001) (**table S2, S8**). The interactors of AtTCP14 are themselves highly connected, mediated largely by three additional AtTCP transcription factors, the foremost being AtTCP13 (**fig. S14**), which itself is targeted 3 times by pathogen effectors (P >0.05; **table S8**). At least AtTCP13 has been identified as an interactor of a histidine-containing phosphotransmitter, and appears to be involved in signal transduction (*74*). Interactors of AtTCP13 are statistically enriched in proteins involved in "regulation of biosynthesis" (adjusted P value = 0.07).

AtTCP transcription factors function via interactions with diverse proteins, e.g. ribosomal subunits, and other transcription factors. AtTCP transcription factors are involved in regulation of diverse processes, in different organelles and by multiple biochemical mechanisms. For a more comprehensive review on AtTCP transcription factors see (*74*). It is hypothesized that AtTCP interact with other transcription factors (TFs) in a regulatory network (*74*). In AI-$1_{MAIN,}$ AtTCP14 interacts with TFs like MAF1 (Mads Affecting Flowering 1), SNZ (Schnarchzapfen), KNAT7 (Knotted-like 7), and APL (Altered Phloem Development). The phenotypes of these proteins agree well with the previously described role for AtTCP14 in development and differentiation (*74*). Another transcription factor interacting with AtTCP14 is WRKY36, a member of the immune function related WKRY transcription factor family. Expression of WRKY36 is differentially regulated upon pathogen infection (*75*).

Primary triggers of effector injection into the plant cytosol are conditions of low sugar and low pH (*76*), suggesting that effectors function to redirection nutrients to the pathogen. Metabolic enzymes interacting with AtTCP14 may act as co-regulators of AtTCP14 that are involved in overall metabolic homeostasis of the host cell.

Elevated calcium and activation of kinase signaling are primary signals of the Microbe-Associated-Molecular-Pattern (MAMP) triggered immunity (MTI) (*77*). Five kinases and four proteins with a role in Ca^{2+} signaling interact with AtTCP14. AtTCP14 may receive signals from these proteins. As such, disruption of AtTCP14 function might be one mechanism of interference with MTI.

Increase of reactive oxygen species is one of the first responses after detection of bacteria via MTI (*2*, *3*, *37*, *38*). The fact that AtTCP14 interacts with nine proteins

involved in RedOx maintenance, and the fact that several of these have additional links to other AtTCP family members, suggests that these enzymes could act as transcriptional co-factors.

Bacterial effectors are targeted to chloroplasts thus indicating the importance of chloroplast processes for infection; however the reasons for this connection are currently unclear (*16*). Seven chloroplast proteins interact with AtTCP14 and photosynthesis proteins are enriched among the AtTCP14 interactors (P = 0.007, one-sided Fisher's exact test). Importantly, for several AtTCP transcription factors, including AtTCP13, both a nuclear (*74*) and chloroplast (*74*) localization has been documented.

RNA binding and processing proteins constitute a large fraction of AtTCP14 interactors. As for RedOx proteins, several RNA processing proteins also interact with other AtTCP family members supporting the functional relevance of these interactions. The RNA-binding protein GRF7 was shown to be a functionally important effector target demonstrating the importance of perturbing RNA function for infectiousness (*16*). The recent finding that animals use bacterial mRNA to detect viable prokaryotes (*78*) opens the exciting possibility that some of the identified RNA binding proteins may act as mRNA sensors.

Altogether, the AtTCP14 function in plant defense that we describe (**Fig. 4**) seems consistent with its local subnetwork composition.

CSN5a (AT1G22920)

CSN5a is a member of the COP9 Signalosome complex, to which effectors from both pathogens together make 23 connections (P <0.001) (**table S2, S8**). A complex assembly of proteins involved in a diversity of different functions forms the CSN5a subnetwork (**fig. S15**). Prominent in this network is a cluster of highly interconnected proteins that correspond to other subunits of the signalosome complex, thus reinforcing the validity of the interactions.

Other interactors of CSN5a are involved in metabolism, RNA-binding, maintenance of RedOx homeostasis and chloroplast function. Interestingly, it has been proposed that some CSN subunits may play an active role in chromatin remodeling, a hypothesis for which interactions of other chromatin remodeling factors (transcriptional regulation in **fig. S15**) with nuclear factors lends support (*79*). In the AI-1_{MAIN} dataset, we observed two full length NB-LRR proteins interacting with CSN5a, supporting the hypothesis that CSN5a is a protein guarded by inactive R proteins, which may become activated upon modification. Alternatively, these proteins may interact with CSN5a on their way to degradation.

For CSN5a, clear independent evidence for a functional role during infection by another class of pathogens comes from a recent study of Geminivirus infection of their plant hosts. Lozano-Duran *et al.* describe how Geminiviruses redirect ubiquitination through their C2 virulence protein by interacting with CSN5a and interfering with the derubylation activity of the CSN complex (*31*). Further, we provide clear evidence of a role of CSN5a in bacterial and fungal infection processes (**Fig 4**).

APC8 (AT3G48150)

APC8 is a member of the APC complex, which regulates cell cycle progression by ubiquitination (*80*). APC8 makes 9 connections with effectors from both pathogens (P <0.001) (**table S2, S8**). In AI-1_{MAIN} APC8 binds to four proteins involved in ubiquitination – the canonical function of the APC complex to which APC8 belongs.

Other interactors are predominantly nucleic acid binding proteins, including several subunits of the ribosome and splicing complex. In addition, a large number of chloroplast proteins are interacting with APC8 including three proteins involved in photosynthesis. These connections mirror the analogous observation for the other hubs described here.

Response to Low Sulfur (LSU1, AT3G49580)

LSU1 is a hub_{50} protein targeted by eight effectors from both pathogens (P = 0.002; **tables S2, S8**). The local interactome of LSU1 reflects similar functional groups as the previously discussed significant hub_{50} proteins: DNA and RNA binding, metabolism, RedOx homeostasis and chloroplast localization (**fig. S17)**. Development of hypotheses for this protein is difficult however, as no molecular function has been described for LSU1.

LSU1 interacts with two Jasmonate responsive co-repressors (JAZ1, JAZ9) and with EDS1 (Enhanced Disease Susceptibility 1), deletion of which causes the disease phenotypes. Interestingly, oomycetes like *Hpa* have selectively and independently lost their ability to acquire sulfur and phosphorus (*9*).

Unknown kinesin light chain-related protein (AT3G27960)

AT3G27960 is a hub_{50} protein targeted by six effectors from both pathogens (P = 0.02; **tables S2, S8**). Kinesins are motor proteins that move cargo along microtubule filaments. Cargo transport, whether actin or microtubule associated, plays a crucial role in various plant processes including plant defense. Geminiviral AL1 protein interacts with Arabidopsis GRIMP (Geminivirus Rep-Interacting Motor Protein; a kinesin protein) and it was suggested that AL1-GRIMP interaction may prevent infected cells from undergoing mitosis (*81*). Another study showed that two members of the whirly family of transcription factors, AtWHY1 and AtWHY3 bind and repress AtKP1 (Arabidopsis Kinesin-Like Protein 1) in a salicylic acid treatment-dependent manner (*82*). A loss-of-function mutant of AtWHY1 is compromised in both basal as well as specific disease resistance (*82*). The local interactome of AT3G27960 reflects similar processes as observed previously (**fig. S18)**: DNA and RNA binding, metabolism, RedOx homeostasis and chloroplast localization. AT3G27960 physically interacts with JAZ1, WRKY21, and Ca^{2+}-signaling proteins reflecting physical interactions with immunity related signaling molecules.

Supporting Figures and Legends:

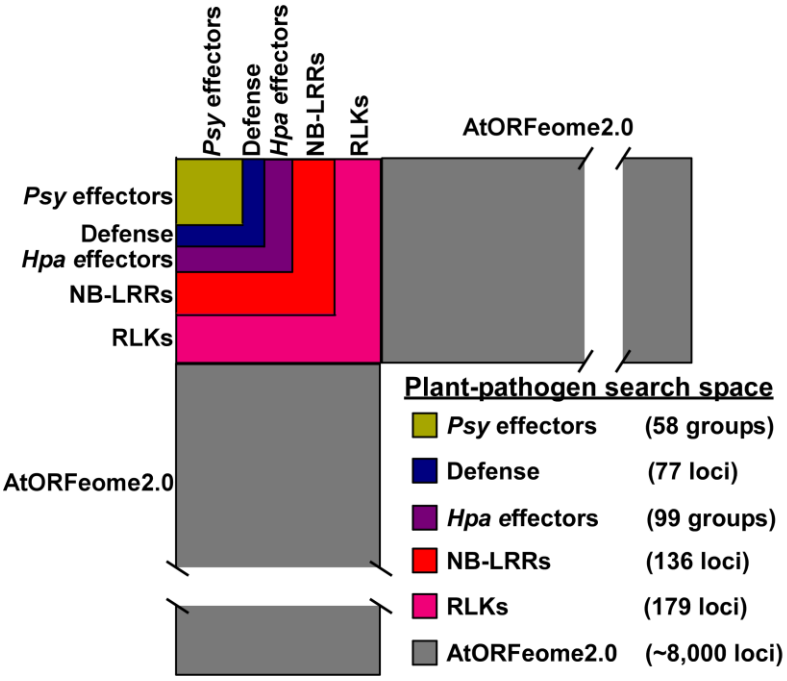

fig. S1. Components used to construct plant-pathogen immune network, version 1 (PPIN-1). Pathogen effectors and plant proteins used as baits to query Arabidopsis AtORFeome2.0 proteins (gray). Effectors were from *P. syringae* (*Psy*; gold) and *H. arabidopsidis* (*Hpa*; purple). Plant proteins including literature-curated defense proteins (blue), N-terminal domains of NB-LRR immune receptors (red), and cytoplasmic domains of LRR-containing receptors like kinase (RLK), a subclass of pattern recognition receptors (pink), were used to map the plant immune network.

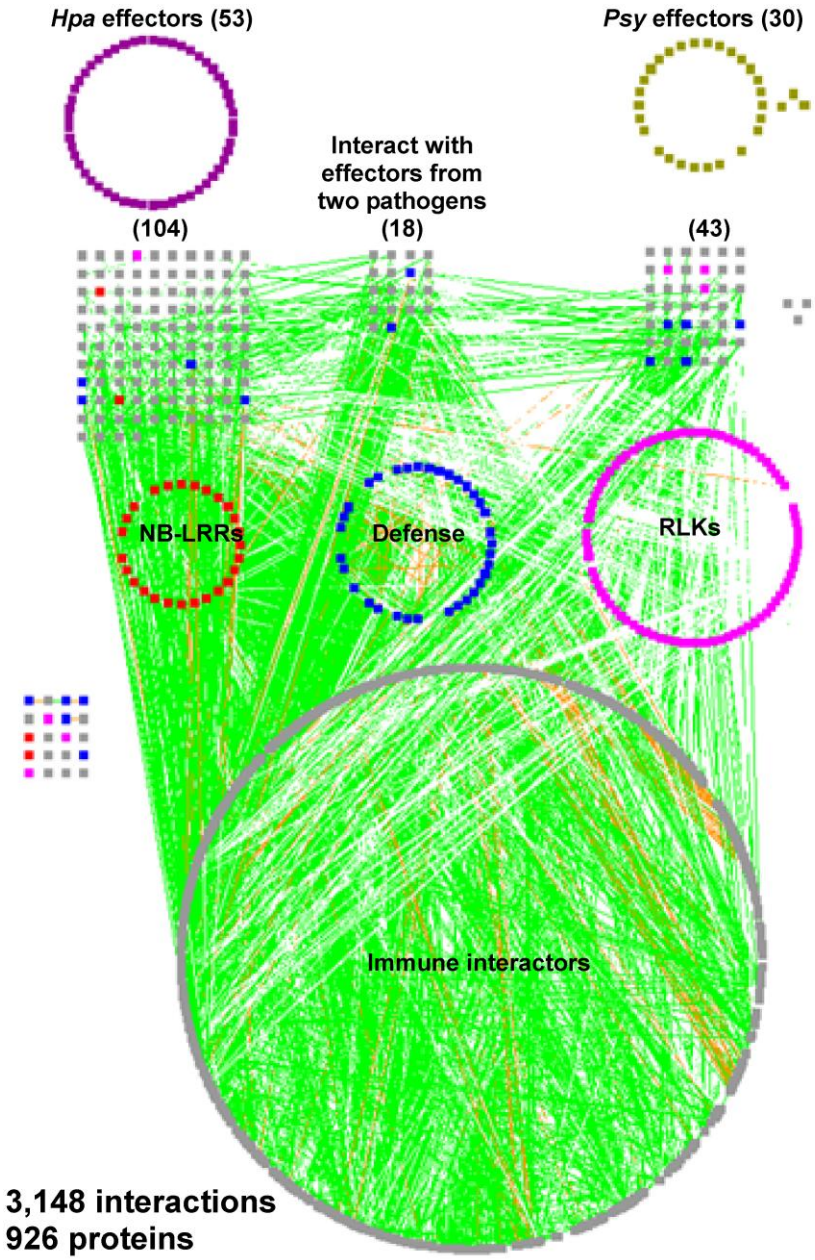

fig. S2. PPIN-1 is densely connected. The network shown in **Fig. 1A** was combined with AI-1 (*11)* and with a compendium of protein interactions assembled from TAIR (*83*), IntAct (*84*) and BIOGRID (*85*) called literature-curated interactions (LCI, see (*11*) for assembly methods). Nodes (representing proteins) are colored according to protein subclasses in **fig. S1**. Number of nodes corresponding to each protein subclass is indicated in parentheses. Edges represent protein-protein interactions. Plant immune interactions (gray edges) from **fig. S1** are omitted in **fig. S2** to emphasize the connectivity acquired. Green edges represent added interactions from AI-1 and LCI. Orange edge: immune, AI-1 and LCI. Individual interactions that are not connected in the layered network involving *Psy* effectors are indicated next to their relevant protein

categories in first and second layers. Grid at left denotes individual interactions involving proteins other than pathogen effectors. Note that the number of individual interactions in the grid is increased in **fig. S2** compared to **Fig. 1A** due to increased connectivity.

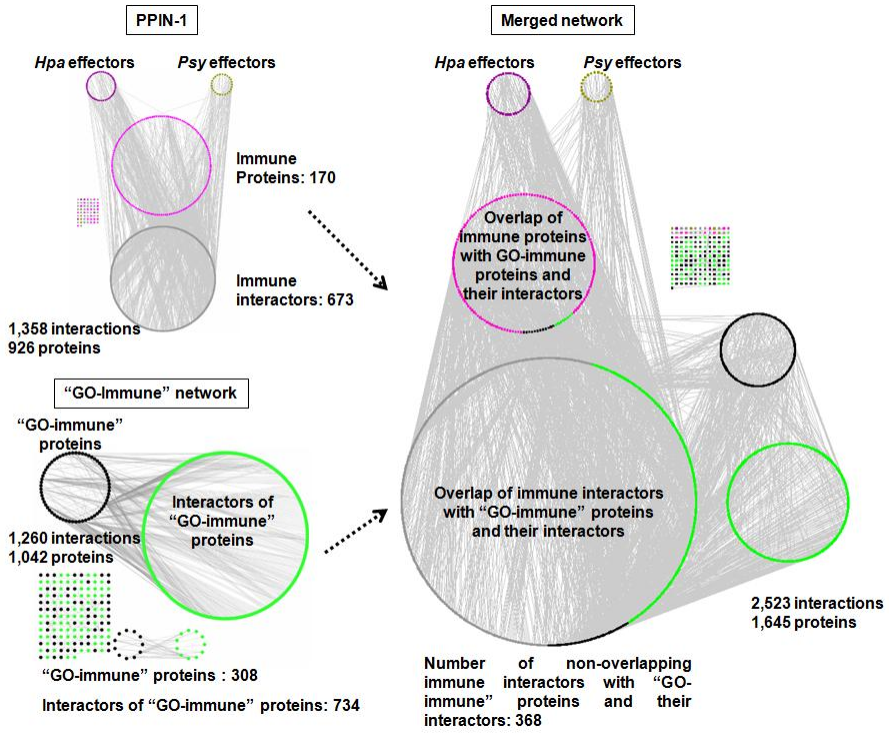

fig. S3. The overlap between plant immune network and "GO-immune" network suggests that at least 368 novel proteins play a role in plant immunity. PPIN-1 (top left panel) is represented here in three layers: effectors of both pathogens (top), plant immune proteins (pink; middle) and the 673 immune interactors from AtORFeome2.0 (gray; bottom). "GO-immune" network (bottom left panel) is derived from 308 AI-1_{MAIN} proteins annotated as "GO-immune proteins" (black; see **table S3**) and their 734 'interactors of GO immune proteins' (green) from AI-1_{MAIN}. Merging of PPIN-1 and the "GO-immune" network (right panel) maps the non-overlapping proteins between the two networks (368). Individual interactions that are not connected in the layered networks are present in a grid beside their respective network.

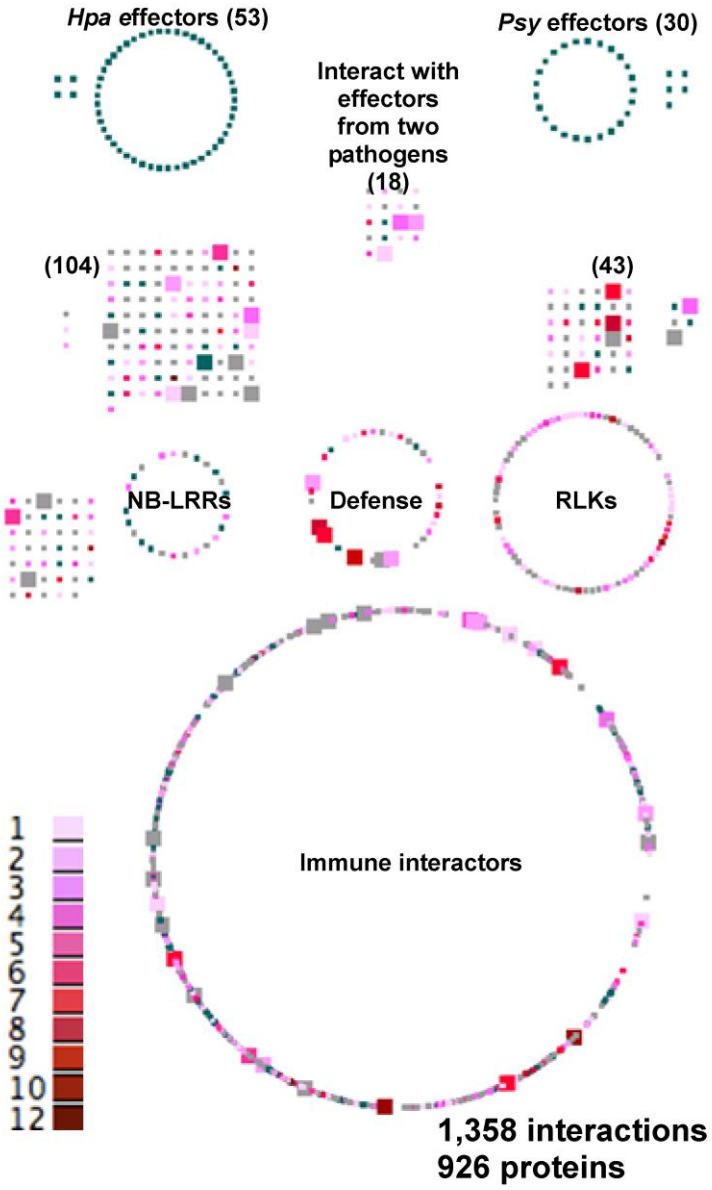

fig. S4. PPIN-1 is enriched in differentially expressed (**DE) genes from defense-related experiments.** PPIN-1 proteins in layered layout (as in **Fig.1A**) but re-colored at a scale from pale pink (1) to dark red (12) according to the number of occurrences of proteins in differentially expressed (DE) gene lists from defense-related transcriptome experiments. Gray: proteins not in DE gene lists. Green: no information present for that particular locus/pathogen effector in defense-related transcriptome. Number of nodes related to several protein sub-classes is listed in parentheses. Larger node squares represent proteins GO annotated as 'hormone response'. Plant immune interactions (gray edges) from **Fig. 1A** are omitted in **fig. S4** to emphasize the node colors and sizes.

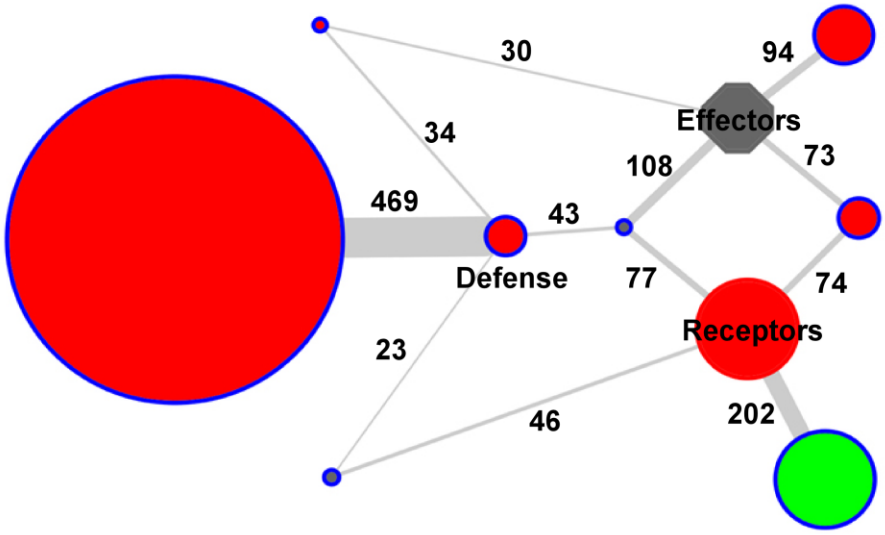

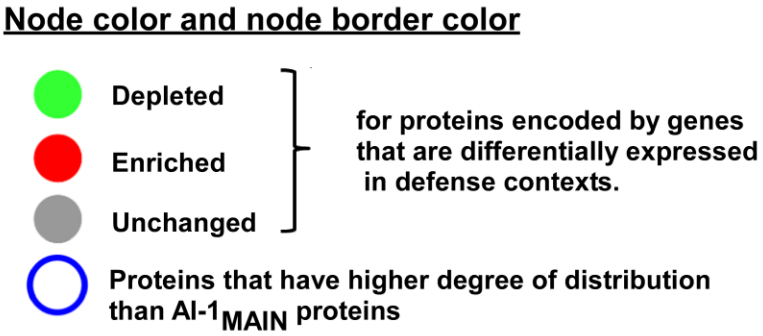

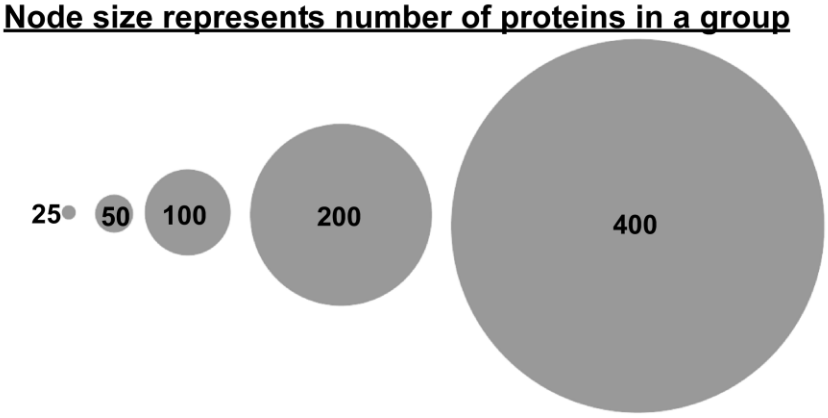

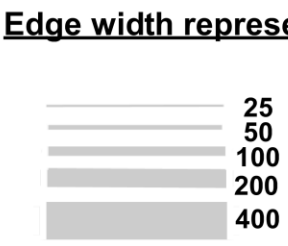

fig. S5. PPIN-1 contains groups enriched and depleted in proteins encoded by genes differentially expressed in defense contexts. Nodes represent subsets of proteins in PPIN- 1 and node size is proportional to the number of proteins in the group.

Nodes are connected by gray edges (numbers of edges given) of width proportional to the number of Y2H interactions. The gray octagonal node represents pathogen effectors, the round nodes Arabidopsis protein groups. Receptors include both NB-LRRs and RLKs. Red nodes are enriched, the green node is depleted, and the gray nodes are unchanged for proteins encoded by genes differentially expressed (DE) in defense contexts. A blue node border signifies that proteins in this group have a significantly higher degree distribution than AI-1_{MAIN} proteins that are not in PPIN-1 (P < 0.05 according to a Mann-Whitney test; (*10*) and **Fig. 2C**), while non-colored node borders indicate few or no proteins from this group are in AI-1_{MAIN} (also see **table S6).**

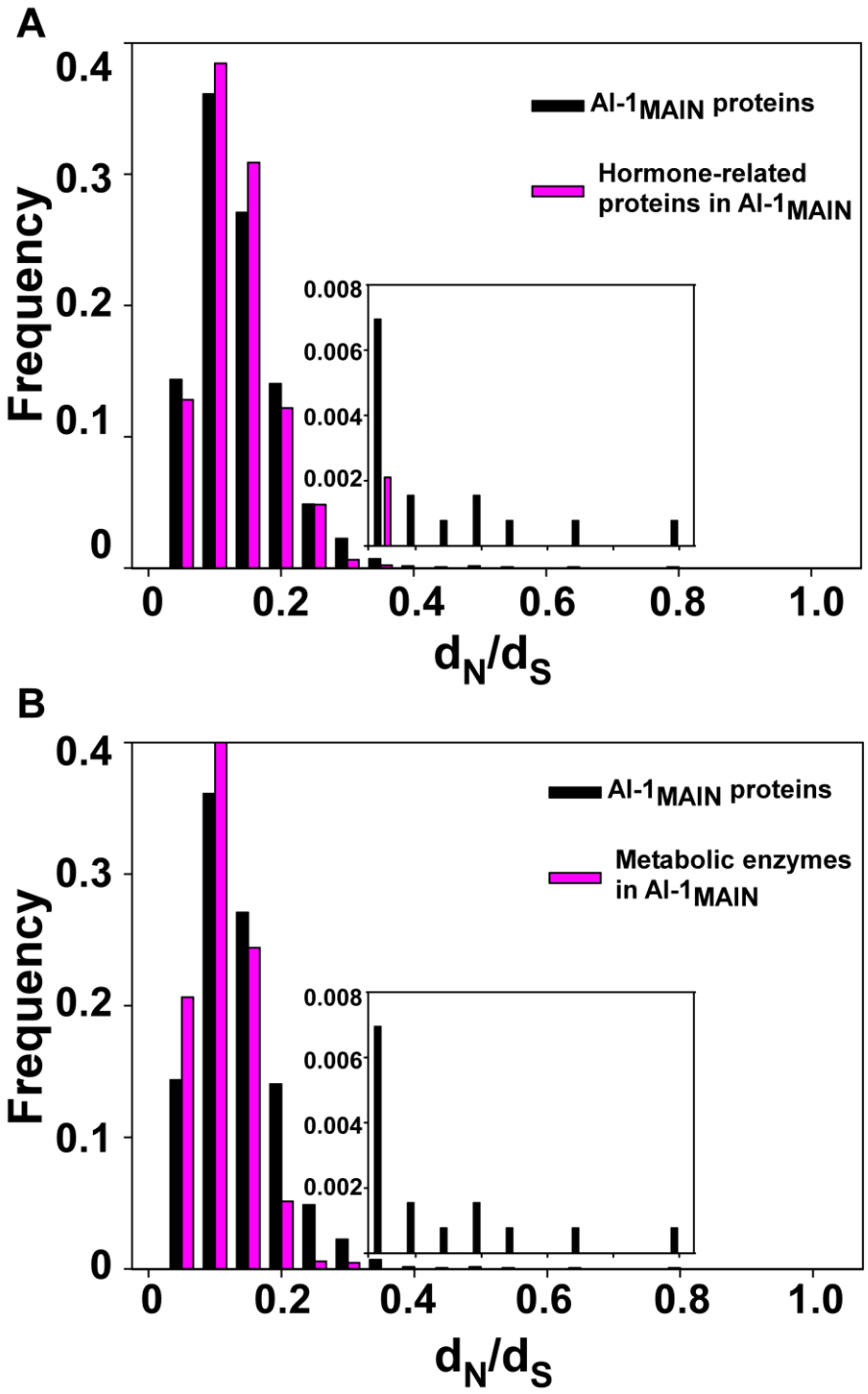

fig. S6. Controls for the evolution rate of PPIN-1 proteins. In order to verify the specificity of our observation that immune interactors in PPIN-1 evolve faster than other proteins in AI-1_{MAIN}, we performed the same analysis on hormone-related proteins (*17)* and metabolic enzymes (*22*). d_N/d_S values were computed between Arabidopsis proteins and their Papaya orthologs. Black and pink bars represent AI-1_{MAIN} and hormone-related **(A)** or metabolic **(B)** proteins, respectively. (**A**) Relative frequency of

d_N/d_S between hormone-related proteins (*17*) in AI-1_{MAIN} and all proteins present in the AI-1_{MAIN} network. A Kolmogorov-Smirnov test shows that these distributions are not statistically different. (**B**) Relative frequency of d_N/d_S between the metabolic enzymes present in AI-1_{MAIN} and all proteins present in the AI-1_{MAIN} network. A Kolmogorov-Smirnov test shows that metabolic enzymes evolve slower than all proteins in AI-1_{MAIN} ($P < 10^{-22}$). Insets are rescaled on the Y-axes to make the higher d_N/d_S categories more apparent. X-axes remain the same for the insets in **A** and **B**.

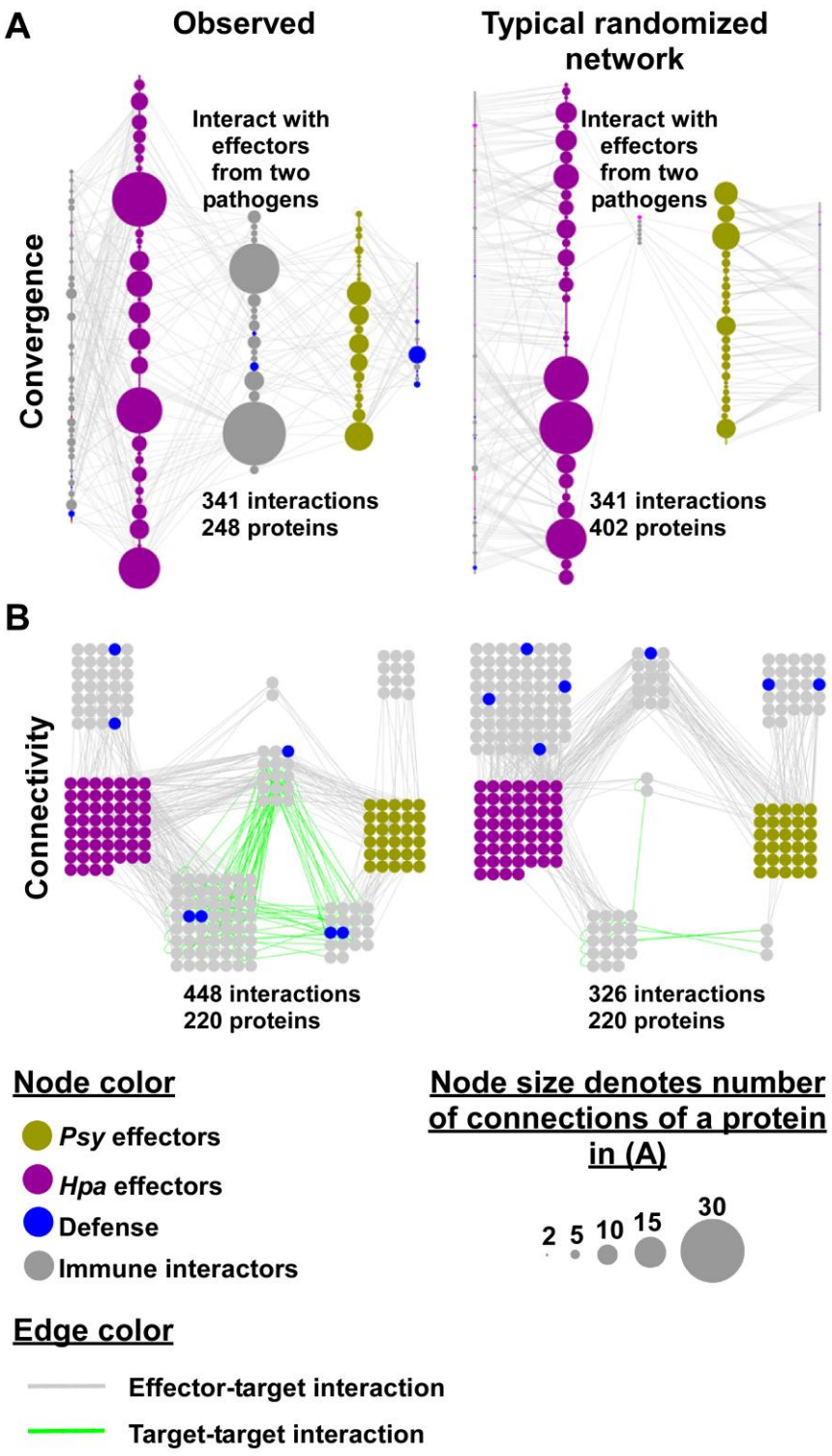

fig. S7. Convergence of pathogen effectors onto interconnected cellular targets. (**A**) Left: observed connectivity between 248 experimentally determined nodes (effectors plus their targets) defines 341 edges. Right: An example of random connectivity (out of

1000 simulations) between the same number of hypothetical effectors with the same degree as the real effectors, and their random targets chosen among proteins present in AI-1 and PPIN-1 required 402 nodes to accommodate the 341 edges. Nodes represent proteins and are colored as in **Fig. 1A, fig. S1**. Gray edges: protein-protein interactions from **Fig. 1A** (left), or their simulated equivalent (right). Node size is proportional to the number of connections made by the node. The smallest node has one interaction =10 (an arbitrary number for size in cytoscape (*62)* and the biggest node has 29 interactions =290. (**B**) Pathogen effector targets are highly interconnected. Left: the observed connectivity in AI-1_{MAIN} between effectors plus their targets present in AI-1 is 220 nodes defining 448 edges. Right: an example of random connectivity (out of 15,000 simulations) in AI-1_{MAIN} between targets of pathogen effectors generates only 326 edges with the same 220 nodes. Nodes represent proteins and are colored as in **Fig. 1A, fig. S1**. Gray edges: protein-protein interactions from **Fig. 1A** (left) or their simulated equivalent (right). Green edges: protein-protein interactions from AI-1_{MAIN} (left), or their simulated equivalent (right).

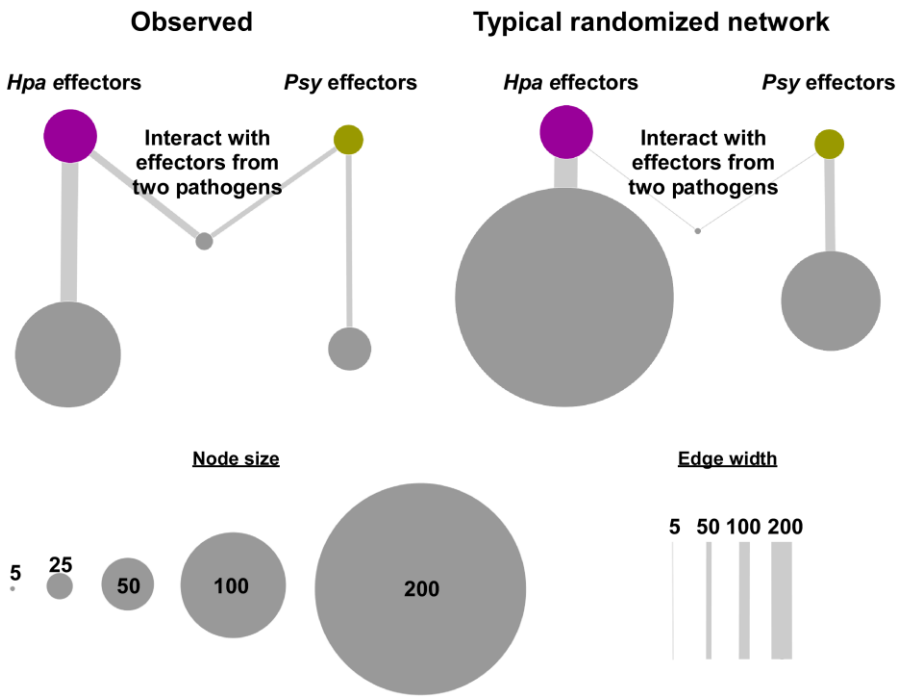

fig. S8. Schematic of effector protein convergence onto interconnected cellular hubs. Experimentally determined (left panel) and randomized (right panel) interactome networks are illustrated. Nodes represent collection of proteins in each category from **fig. S7A**. Edges represent collection of protein-protein interactions between two nodes.

A

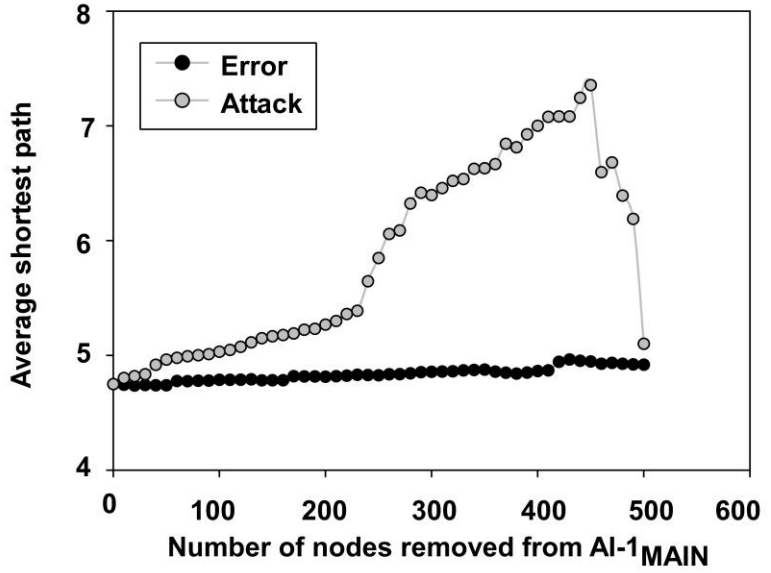
Error
Attack
Average shortest path
8
7
6
5
4
0
100
200
300
400
500
600
Number of nodes removed from AI-1MAIN

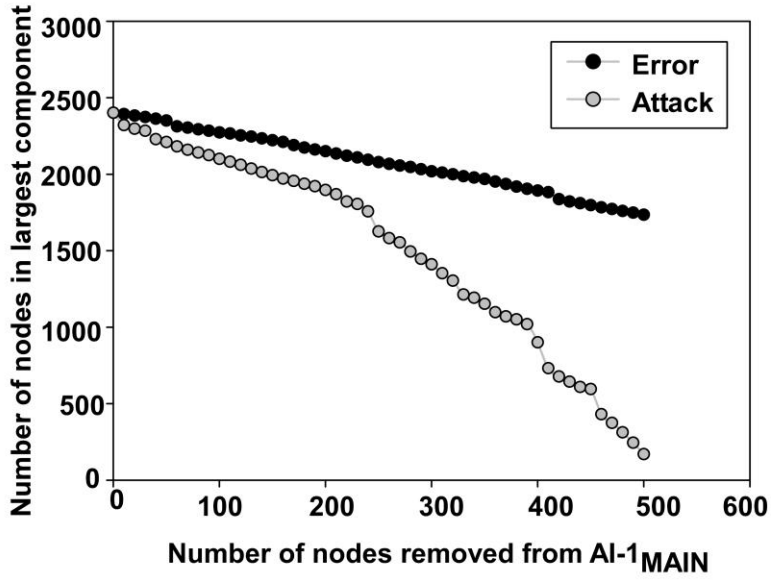
Error
Attack
Number of nodes in largest component
3000
2500
2000
1500
1000
500
0
0
100
200
300
400
500
600
Number of nodes removed from AI-1MAIN

B

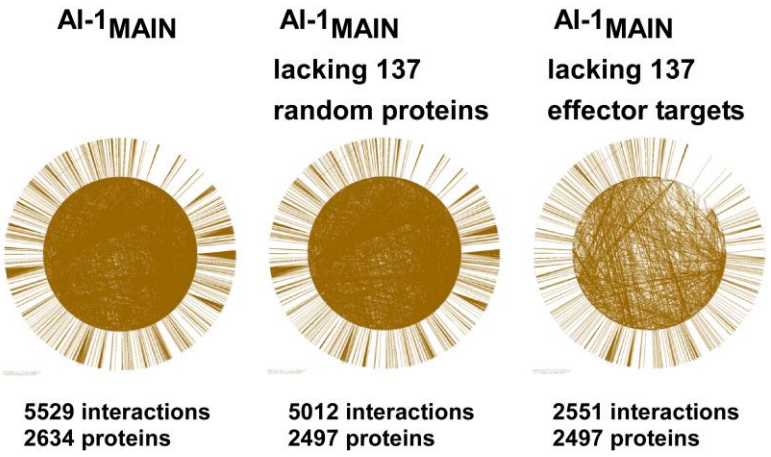
AI-1MAIN
AI-1MAIN lacking 137 random proteins
AI-1MAIN lacking 137 effector targets
5529 interactions
2634 proteins
5012 interactions
2497 proteins
2551 interactions
2497 proteins

fig. S9. Computational simulations of targeted attacks and random failures on AI-1_{MAIN}. (**A)** Evolution of the average shortest path (top panel) and the number of nodes in the largest component (bottom panel) upon random removal of the same number of nodes, either chosen among all nodes ("errors") or only among the nodes of degree ≥5 ("attacks"). These simulations show that AI-1_{MAIN} shares the property of scale-free networks to be resistant to random errors but sensitive to targeted attacks of their hubs. (**B)** Circular representation of AI-1_{MAIN} (left), AI-1_{MAIN} after removal of 137 random nodes and the corresponding edges (middle), AI-1_{MAIN} after removal of the 137 effector targets identified in PPIN-1 that are also present in AI-1_{MAIN} and the corresponding edges (right). All nodes represent proteins and are arranged in a circle; all edges represent interactions; all self-interaction loops are eliminated.

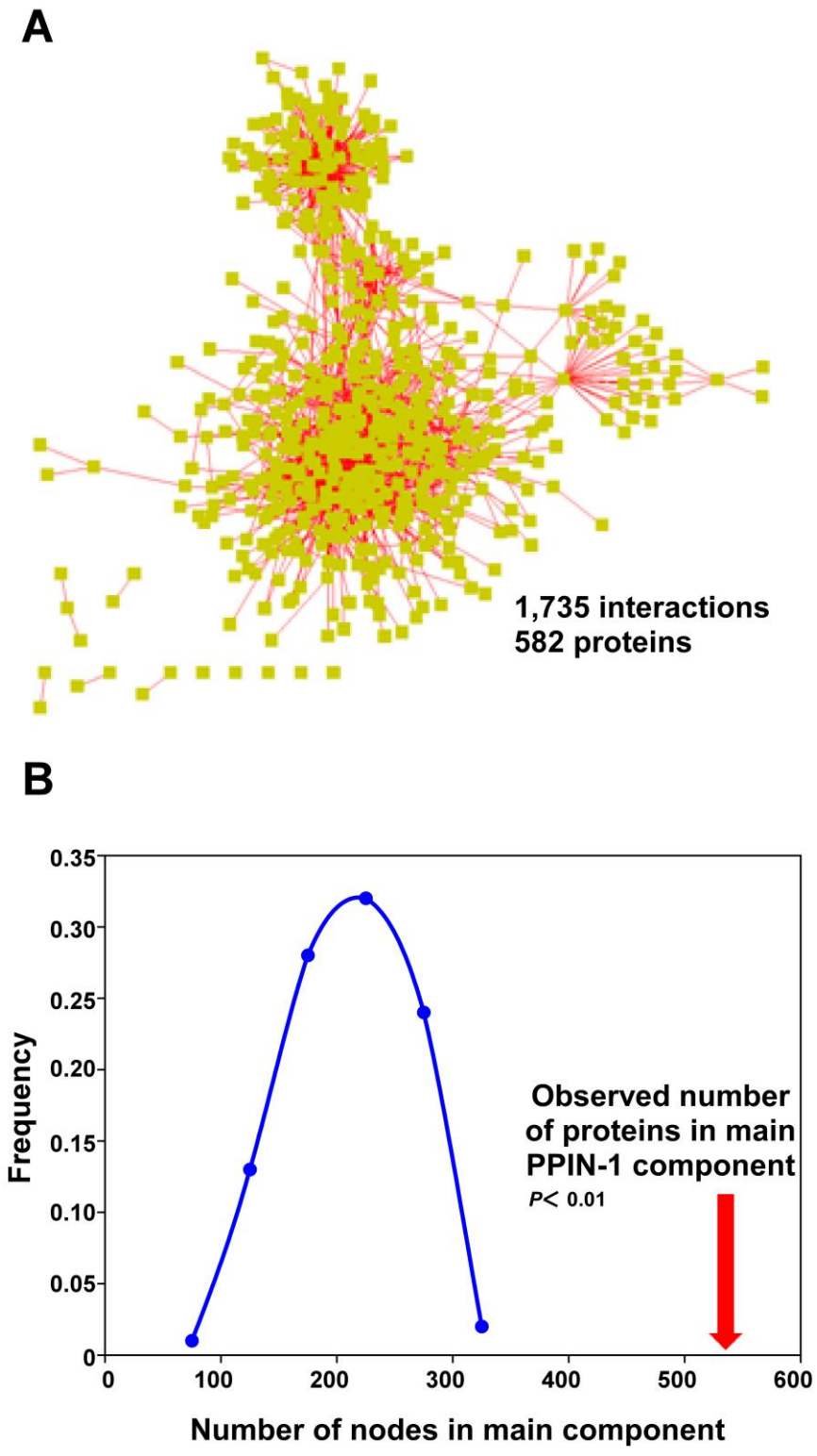

fig. S10. Proteins in PPIN-1 are densely connected in AI-1_{MAIN}. To evaluate the extent to which the proteins of the plant immune network were connected in the AI-1_{MAIN}, we calculated that the 632 proteins present in PPIN-1 and also present in AI-1_{MAIN}

formed a subnetwork of 582 proteins including 566 forming a single component. We then performed 100 random selections of 632 proteins in AI-1_{MAIN} and measured the number of nodes of the largest components of these random controls. This number never reached 566 making the empirical *P*-value for our observation < 0.01. (**A**) A sub network of AI-1_{MAIN} containing 582 PPIN-1 proteins (node; gold) and 1735 Y2H interactions (edges; red) includes 566 nodes and 1723 edges in a single component. (**B**) The graph shows the number of nodes forming the largest component of 100 bootstrapped networks generated by selecting 632 proteins randomly from AI-1_{MAIN} (bottom); the red arrow indicates the observed number of PPIN-1 nodes in the largest component: 566 (*10*).

A

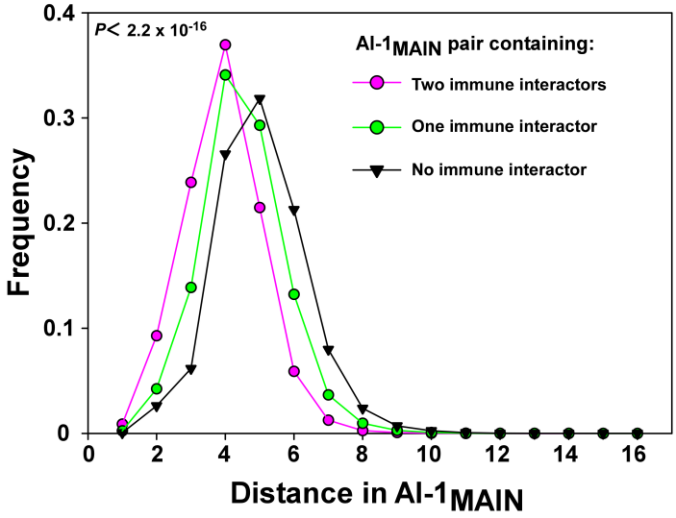
P< 2.2 x 10-16
Al-1MAIN pair containing:
Two immune interactors
One immune interactor
No immune interactor
Frequency
Distance in Al-1MAIN

B

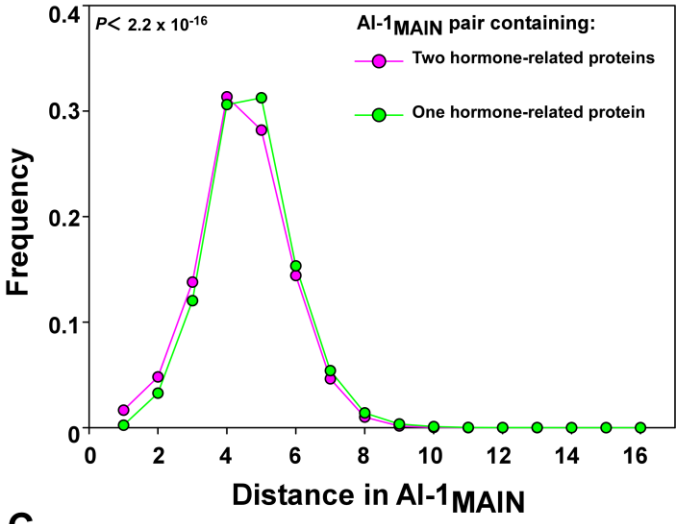
P< 2.2 x 10-16
Al-1MAIN pair containing:
Two hormone-related proteins
One hormone-related protein
Frequency
Distance in Al-1MAIN

C

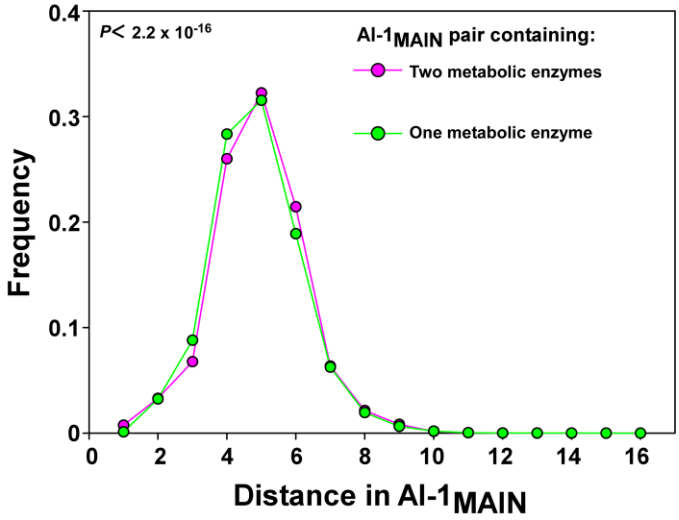
P< 2.2 x 10-16
Al-1MAIN pair containing:
Two metabolic enzymes
One metabolic enzyme
Frequency
Distance in Al-1MAIN

fig. S11. Proteins in PPIN-1 are close to each other in AI-1_{MAIN}. We considered 3 groups of proteins in AI-1_{MAIN}: i) Immune interactors present in both PPIN-1 and AI-1_{MAIN}, ii) hormone-related proteins (*17*), and iii) metabolic enzymes (*22*). For each of these groups, we compared the distribution of pairwise shortest paths in AI-1_{MAIN} for pairs of proteins within the group (pink), to pairs consisting of one protein of the group and one other protein in AI-1_{MAIN} (green) and protein pairs from the remaining of AI-1_{MAIN} (black). (**A**) Immune interactors present in AI-1_{MAIN}. The distances between proteins in the first group are significantly shorter than those in the second group according to a Mann Whitney test ($p < 2.2e^{-16}$). In black is the distribution of pairwise shortest paths in AI-1_{MAIN} for protein pairs that are not present in PPIN-1. (**B**) Hormone-related proteins. The distances between proteins in the first group are significantly shorter than those in the second group according to a Mann Whitney test ($P < 2.2e^{-16}$), but to a lesser extent than in (**A**). (**C**) Metabolic enzymes. The distances between proteins in the first group are significantly longer than those in the second group according to a Mann Whitney test ($P < 2.2e^{-16}$).

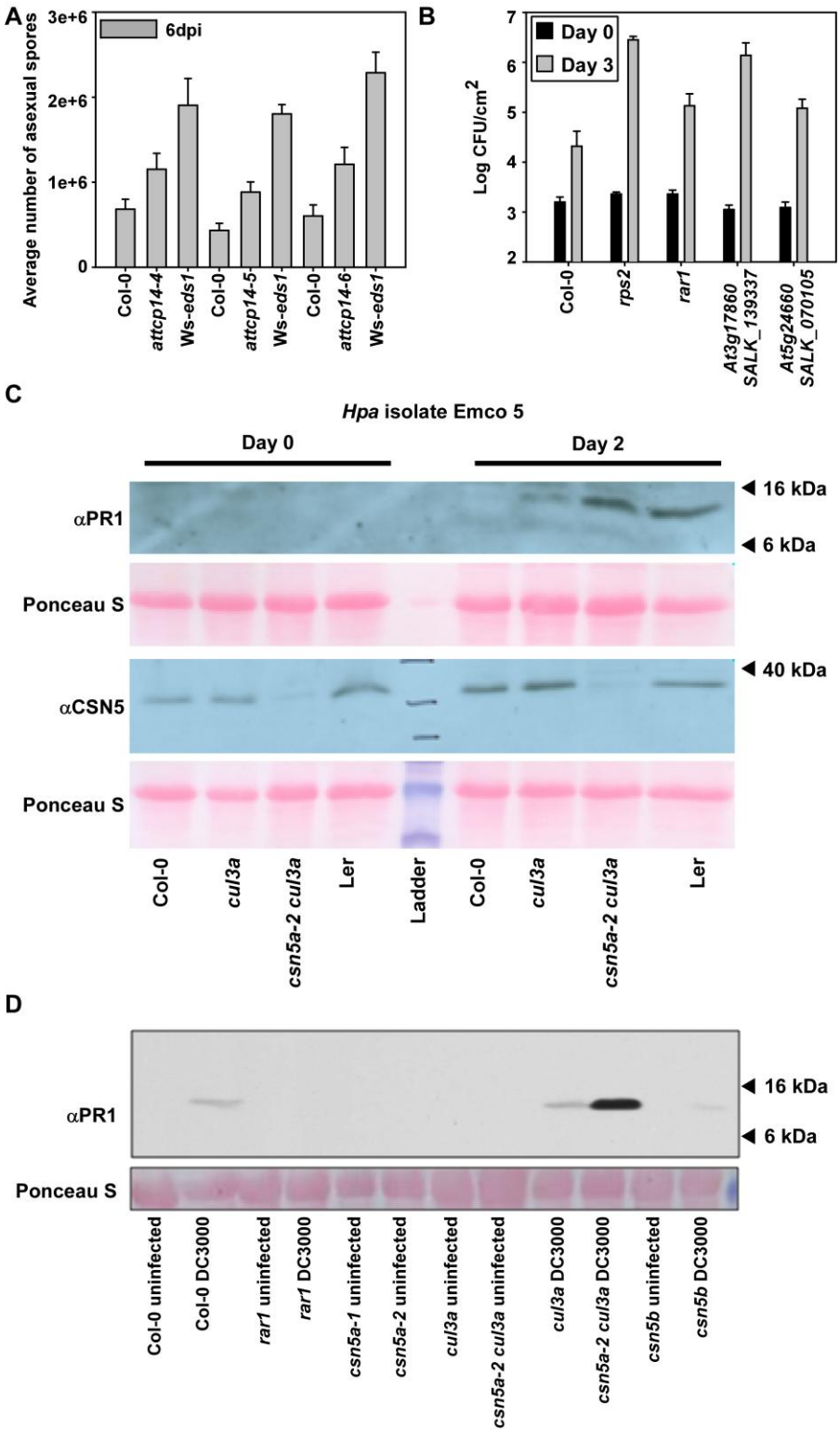

fig. S12. Target validation: Function of AtTCP14, CSN5, At3g17860 and At5g24660 in plant defense. (**A**) Loss-of-function *attcp14* mutants (three independent alleles as designated) also exhibit enhanced susceptibility to *Hpa* isolate Noks1. Average number

of asexual spores formed 6 dpi in the indicated genotypes was determined Col-0 (susceptible) and Ws-*eds1* (*e*nhanced *d*isease *s*usceptibility) genotypes are used as controls. Error bars represent average ± SE of six replicates ($P < 0.05$ according to a Mann-Whitney test). (**B**) *P. syringae* DC3000(*avrRpt2*) growth (colony forming unit – CFU/cm^2, expressed on a log scale) in leaves of the indicated genotypes at bottom. Bacterial growth was assessed at 3 dpi. Loss of function *rps2* and *rar1* (compromised in both ETI and MTI) mutants were used as controls. Error bars represent the mean ± two times standard error of four replicates. RPS2 function was chosen since, like RPP4 function tested in **Fig. 4A**, it is partially SA-dependent. Neither At3g17860 nor At5g24660 has been previously implicated in RPS2 function. Because our bacterial growth assays are less sensitive than precise counting of *Hpa* sporangiophores, we expected that the modest *eds* and *edr* phenotypes shown in **Fig. 4, A and B** would be difficult to observe with bacterial population measurements. Nevertheless these preliminary observations support the general conclusion of **Fig. 4** and suggest detailed follow up experiments. (**C**) Western blots with anti-PR1 and anti-CSN5 on crude leaf extract of the indicated genotypes from untreated and infected with *Hpa* Emco5 for 2 days. Ponceau S stain verifies equal loading. (**D**) PR1 protein hyper-accumulates after infection in the *csn5a-2 cul3* double mutant. Total protein extracts of uninfected tissue or from tissue harvested 2 days after inoculation with *P. syringae* DC3000 were probed with an anti-PR1 antibody. Ponceau S stain verifies nearly equal loading. Note the absence of ectopic PR1 expression before infection in (**C**) and (**D**).

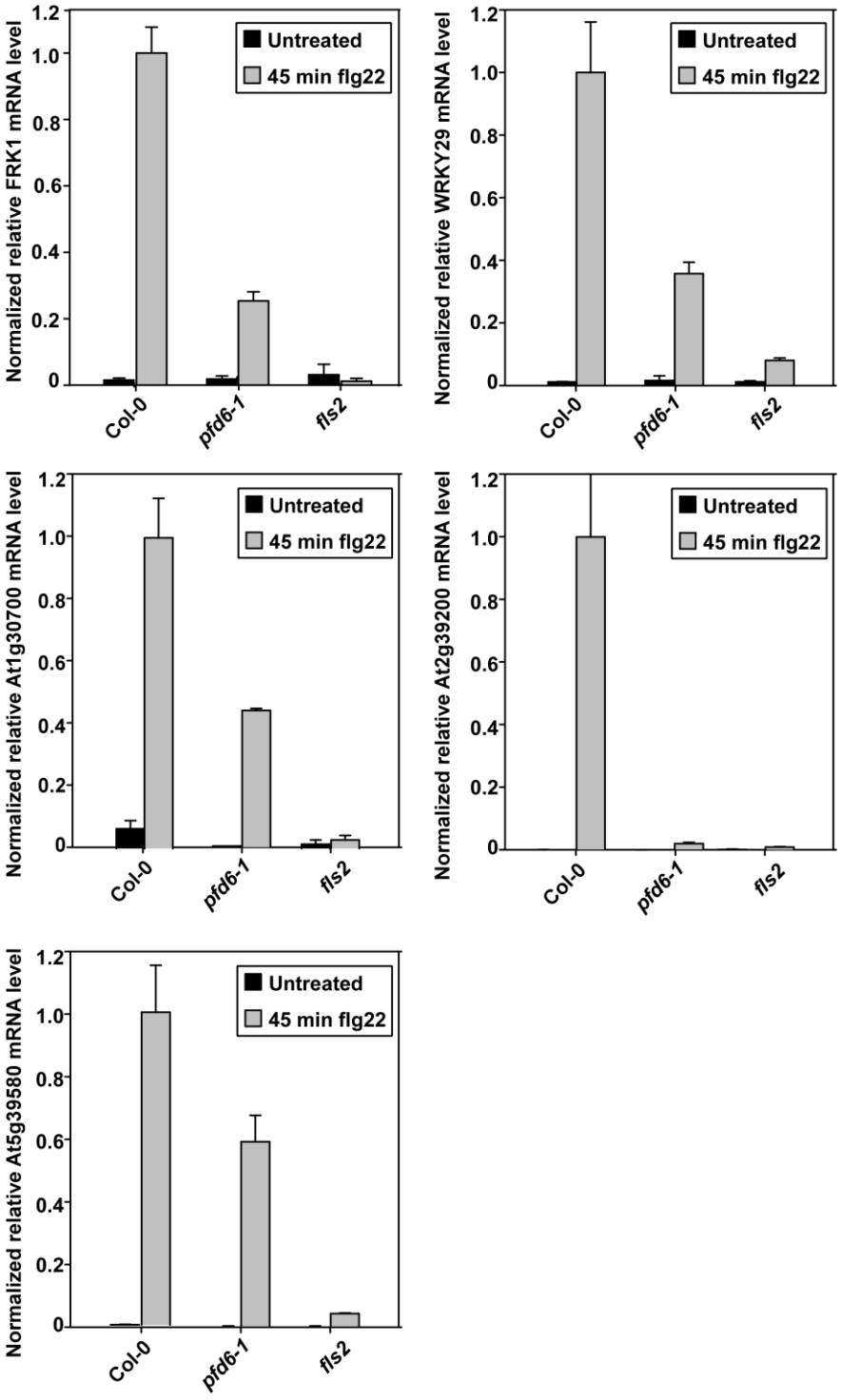

fig. S13. Expression of MTI-responsive genes in *pfd6-1*. Relative transcript levels of MTI responsive genes were determined by quantitative RT-PCR using cDNA generated from leaves treated with flg22 for 45min. The expression values were normalized using the expression level of the UBQ5 as an internal standard. Normalized values of

indicated MTI responsive genes in Col-0 are arbitrarily adjusted to 1. Error bars represent average ± standard deviation of at least two replicates.

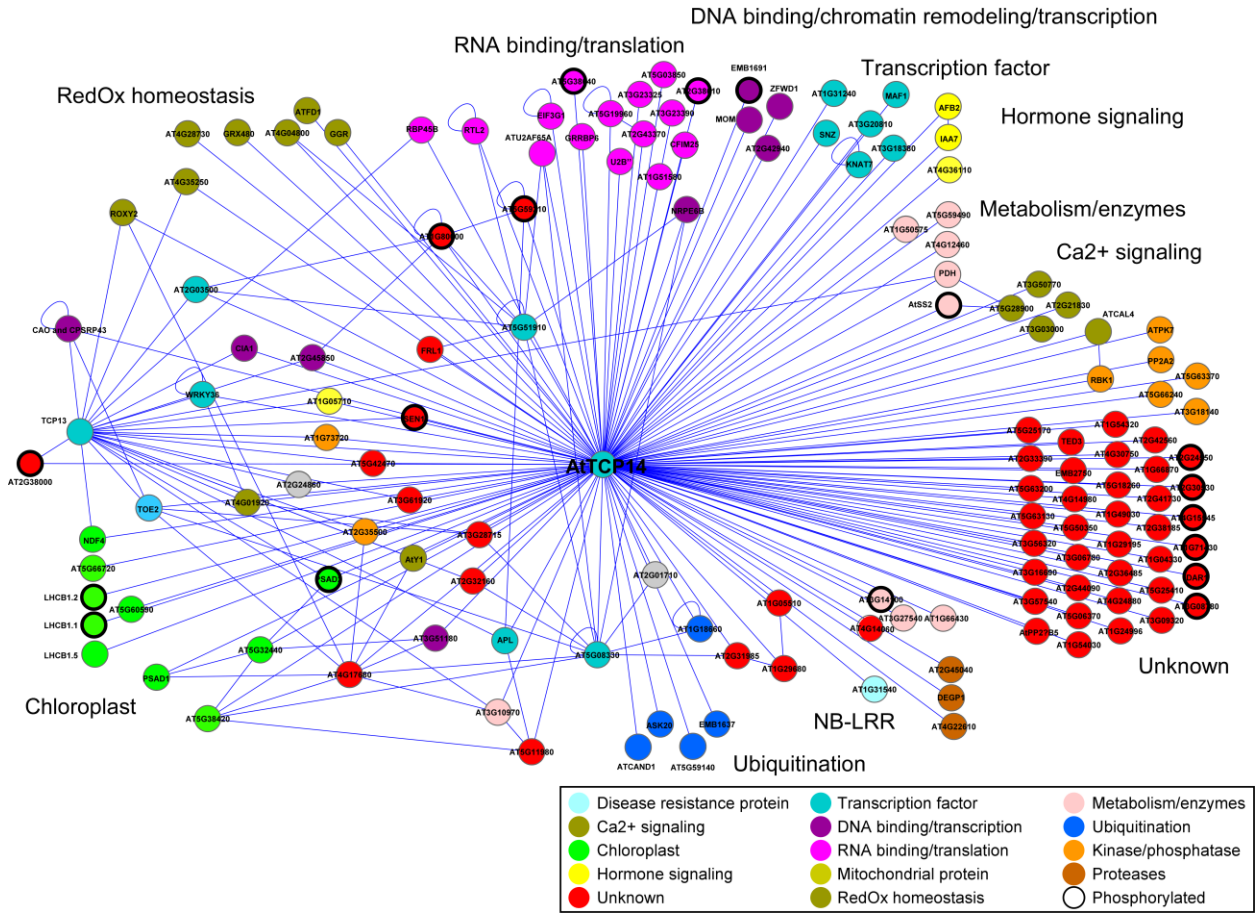

fig. S14. Local interactome of AtTCP14 (AT3G47620) and interacting proteins.

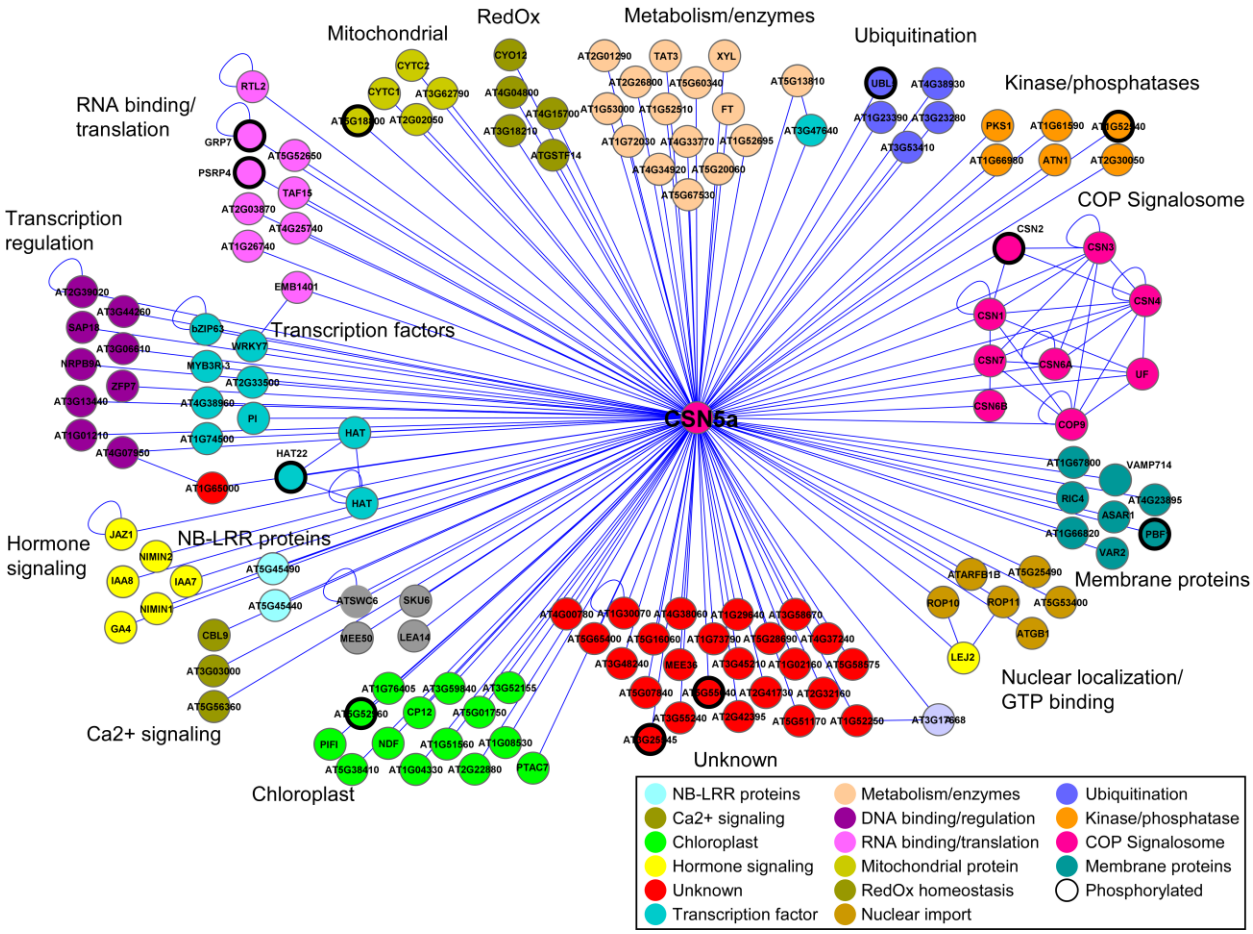

fig. S15. Local interactome of CSN5a (AT1G22920) and interacting proteins.

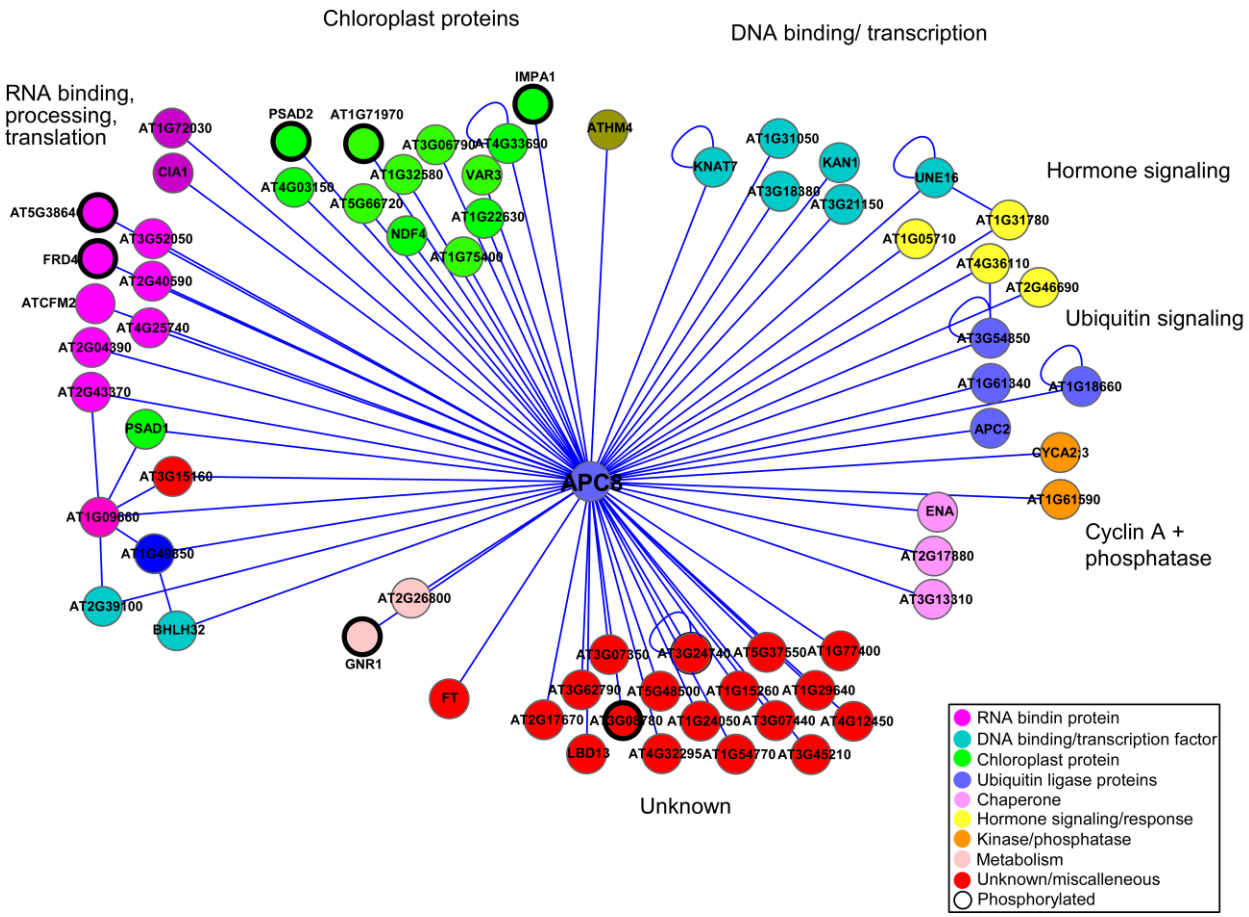

fig. S16. Local interactome of APC8 (AT3G48150) and interacting proteins.

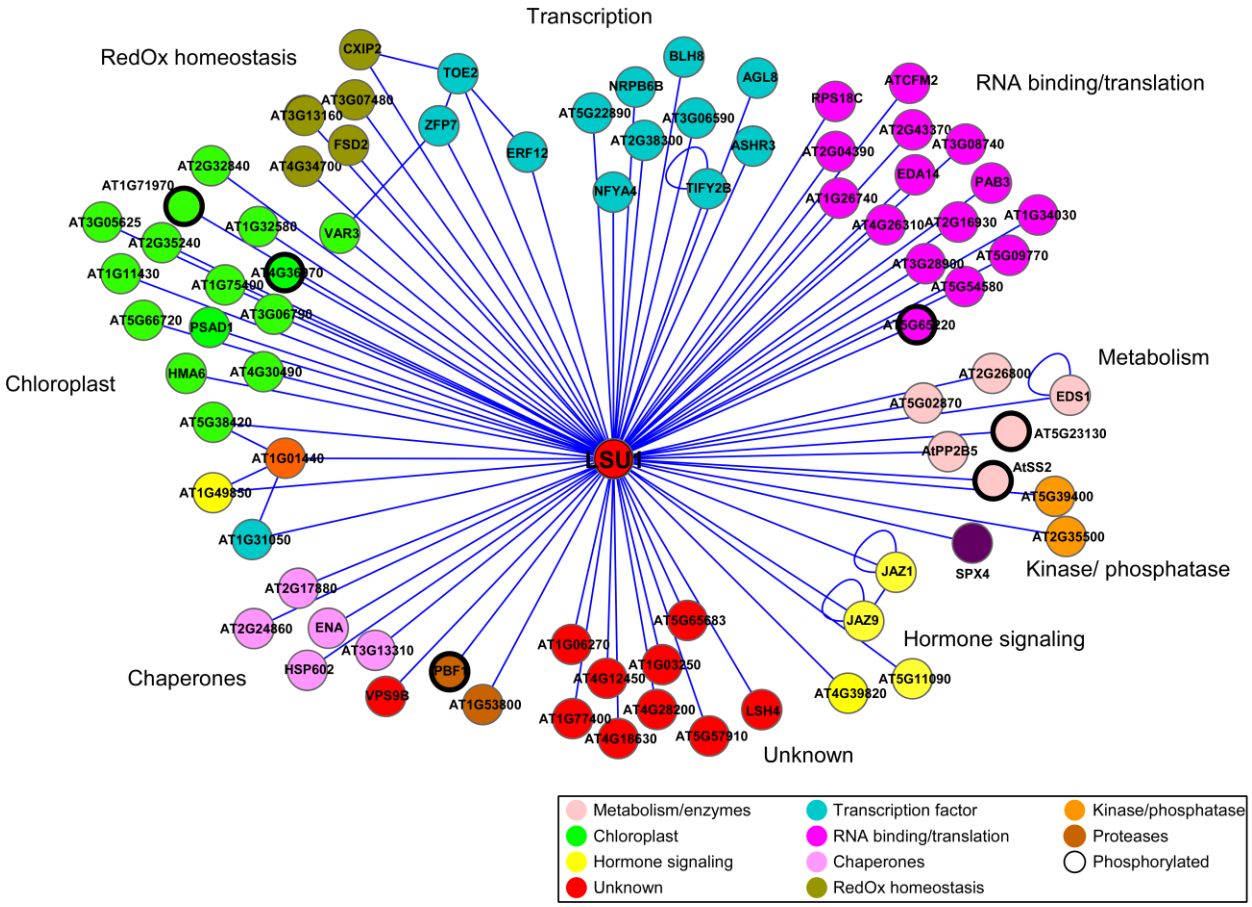

fig. S17. Local interactome of LSU1 (AT3G49580) and interacting proteins.

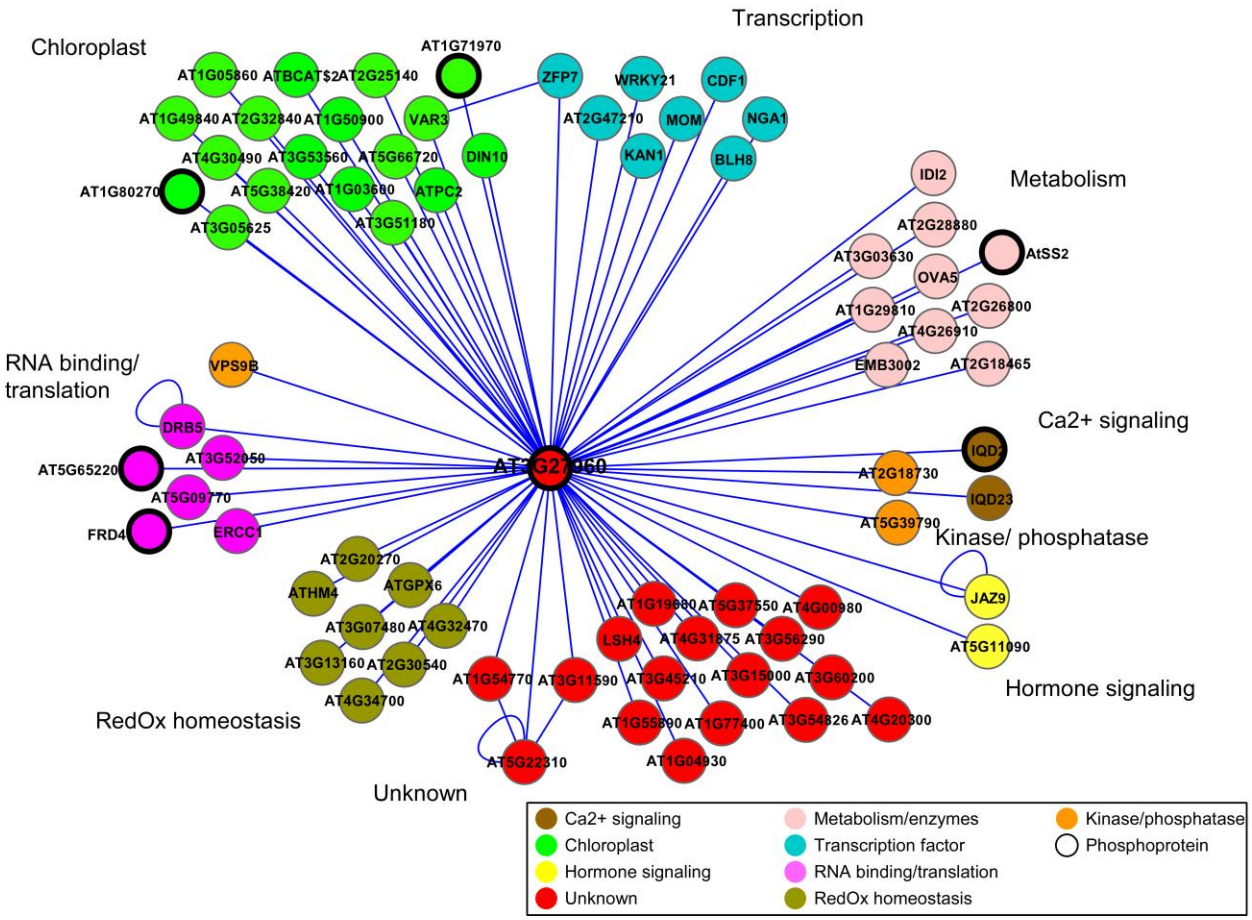

fig. S18. Local interactome of unknown kinesin light chain-related protein (AT3G27960) and interacting proteins.

table S3. List of immune-related GO-terms	
GO_id	**GO_name**
GO:0002218	activation of innate immune response
GO:0002376	immune system process
GO:0002682	regulation of immune system process
GO:0006915	apoptosis
GO:0006950	response to stress
GO:0006952	defense response
GO:0006955	immune response
GO:0007169	transmembrane receptor protein tyrosine kinase signaling pathway
GO:0008219	cell death
GO:0009408	response to heat
GO:0009409	response to cold
GO:0009607	response to biotic stimulus
GO:0009617	response to bacterium
GO:0009814	defense response, incompatible interaction
GO:0009816	defense response to bacterium, incompatible interaction
GO:0009862	systemic acquired resistance, salicylic acid mediated signaling pathway
GO:0009867	jasmonic acid mediated signaling pathway
GO:0045087	innate immune response
GO:0048583	regulation of response to stimulus
GO:0071216	cellular response to biotic stimulus

table S4. Enrichment and depletion statistical tests

1- The overlap between immune interactors and GO-immune proteins in AtORFeome2.0 is not larger than expected from random sampling (p-value= 0.075)

counts in all AtORFeome2.0 (8430 proteins)

	immune interactor	not immune-interactor
go-immune	66	909
not go-immune	607	6848

2- Effector targets are enriched in GO-immune proteins (p-value= 0.03)

counts among immune interactors only (673 proteins)

	target	non-target
immune	21	45
non immune	127	480

3- Effector targets are enriched in hormone-related proteins (p-value= 0.01)

counts among immune interactors only (673 protens)

	target	non-target
hormone-related	18	31
not hormone-related	130	494

4- common targets of the effectors of two pathogens are enriched in hubs with more than 50 interactors (p-value= 6.5 e-13)

counts among all AI-1MAIN proteins (2661 proteins)

	target of 2 pathogens	not target of 2 pathogens
more than 50 interactors	7	8

less than 50 interactors	10	2636

5- Effector targets are enriched in hubs with more than 50 interactors (p-value = 6.9 e-18)

counts among all AI-1MAIN proteins (2661 proteins)

	target	non-target
more than 50 interactors	14	123
less than 50 interactors	1	2523

6- Significant targets are enriched in hubs with more than 50 interactors (p = 5e-6)

counts among all AI-1MAIN proteins (2661 proteins)

	significant target	not significant target
more than 50 interactors	5	10
less than 50 interactors	46	2600

7-Significant common targets of the effectors of two pathogens are enriched in hubs with more than 50 interactors (p-value= 0.006)

counts among all significant targets (51 proteins)

	significant target of 2 pathogens	significant target of 1 pathogen
more than 50 interactors	4	1
less than 50 interactors	7	39

8- Common targets of the effectors of two pathogens are enriched in significant targets (p-value= 0.003)

counts among all targets present in AI-1MAIN (137 proteins)

	target of 2 pathogens	target of 1 pathogen
significant target	12	39

not significant target	5	81

9- Effector targets are depleted in NB-LRRs (p-value= 0.047)

counts among all Arabidopsis proteins in PPIN-1 (843 proteins)

	target	non-target
NB-LRR	2	28
non-NB-LRR	163	650

10- Interactors of NB-LRRs are enriched in effector targets (p-value =4.6e-05)

counts among all immune interactors (673 proteins)

	target	non-target
NB-LRR interactor	24	28
not NB-LRR interactor	124	497

11- Interactors of NB-LRRs are enriched in hubs with more than 50 interactors (p-value=8.e-12)

counts among all AI-1MAIN (2661 proteins)

	more than 50 interactors	not more than 50 interactors
NB-LRR interactor	7	16
not NB-LRR interactor	8	2630

12- Effector targets are depleted in RLKs (p-value=1.6e-05)

counts among all Arabidopsis proteins in PPIN-1 (843 proteins)

	target	non-target
RLK	4	86
non-RLK	161	592

13- Interactors of RLKs are enriched in effector targets (p-value =0.02)

counts among all AtORFeome2.0 proteins in PPIN-1 673 proteins)

	target	non-target
RLK interactor	46	116
not RLK interactor	102	409

14- The effectors targets that are also present in AtORFeome2.0 are enriched in angiosperm-specific genes (p-value = 0.0007)

counts in all AtORFeome2.0 proteins included in ortholog search

	angiosperm specific	more broadly conserved
effector targets	67	76
not effector targets	2744	5450

table S5: GO-term enrichment analyses of effector targets								
attribute.ID	**number of proteins in the set with this GO term**	**total number of protein in the set and in AI-1/MS**	**number of proteins in AI-1/MS with this go term**	**unadj.p.val**	**adj.p.val**	**enrichment**	**GO_type**	**GO_name**
GO:0030528	30	130	274	1.05E-05	0	2.83933	molecular_function	transcription regulator activity
GO:0003677	32	130	318	2.97E-05	0.001	2.58604	molecular_function	DNA binding
GO:0003700	28	130	253	1.81E-05	0.001	2.84399	molecular_function	transcription factor activity
GO:0005488	73	130	1090	0.00024	0.02	1.90263	molecular_function	binding
GO:0050789	36	130	422	0.0003	0.029	2.14408	biological_process	regulation of biological process
GO:0050794	34	130	388	0.00028	0.029	2.19601	biological_process	regulation of cellular process
GO:0005634	35	130	424	0.00072	0.033	2.04474	cellular_component	nucleus
GO:0003676	37	130	460	0.00081	0.059	1.99682	molecular_function	nucleic acid binding
GO:0009725	17	130	147	0.0006	0.086	2.83736	biological_process	response to hormone stimulus
GO:0010556	23	130	231	0.00057	0.086	2.43611	biological_process	regulation of macromolecule biosynthetic process
GO:0009719	18	130	163	0.00072	0.097	2.69723	biological_process	response to endogenous stimulus

GO:0009889	23	130	236	0.00078	0.104	2.37393	biological_process	regulation of biosynthetic process
GO:0031326	23	130	236	0.00078	0.104	2.37393	biological_process	regulation of cellular biosynthetic process
GO:0010468	23	130	241	0.00105	0.142	2.31461	biological_process	regulation of gene expression
GO:0080090	23	130	241	0.00105	0.142	2.31461	biological_process	regulation of primary metabolic process
GO:0060255	23	130	245	0.00132	0.184	2.26907	biological_process	regulation of macromolecule metabolic process

Glossary:

AtORFeome2.0: The Arabidopsis clone collection used for interactome mapping here and in (*11*).

AI-1_{MAIN}: Arabidopsis Interactome, version 1, main set. A dataset of 5,664 protein-protein interactions between 2,661 proteins that was produced by screening all pairwise combinations in AtORFeome2.0 twice.

AI-1: Arabidopsis Interactome, version 1. A composite dataset corresponding to the union of AI-1_{MAIN} and a screen repeated 6 times on 4% of all pairwise combinations in AtORFeome2.0. AI-1 contains 6,205 interactions between 2,774 proteins.

PPIN-1: Plant-Pathogen Immune Network, version 1. All protein-protein interactions between pathogen effector proteins, immune proteins and immune interactors from i) the experimentally determined plant-pathogen immune network (**Fig. 1A**), ii) AI-1, and iii) a set of literature-curated interactions (LCI; see (*11*) for assembly methods). PPIN-1 contains 3,148 interactions between 926 proteins

Immune proteins: A set of 392 proteins related to the plant immune system for which we included clones when mapping PPIN-1. Immune proteins are subdivided in three subclasses: i) N-terminal domains of NB-LRR disease resistance proteins; ii) cytoplasmic domains of LRR-containing receptor like kinases (RLKs), a subclass of pattern-recognition receptors; and (iii) known signaling components or targets of pathogen effectors (defense proteins) (**fig. S1**, **table S1,** *10*). PPIN-1 contains 170 immune proteins, represented in the third layer from the top in **Fig. 1A** and **fig. S2**.

Immune interactors: A set of 673 proteins that interact with at least one immune protein or one pathogen effector protein in PPIN-1. 148 of the immune interactors are also effector targets. In total, 602 immune interactors are also present in AI-1_{MAIN}.

Effector targets: A set of 165 proteins that interact with at least one pathogen effector protein in PPIN-1. 148 of the effector targets are immune interactors and 17 are immune proteins. In total, 137 effector targets are present in AI-1_{MAIN} among which 51 interact with more effector proteins that would be expected based on their degree in AI-$1_{MAIN.}$ The latter are referred to as “significant targets”.

References and Notes

1. C. Zipfel, Early molecular events in PAMP-triggered immunity. *Curr. Opin. Plant Biol.* **12**, 414 (2009). doi:10.1016/j.pbi.2009.06.003 Medline

2. T. Boller, S. Y. He, Innate immunity in plants: An arms race between pattern recognition receptors in plants and effectors in microbial pathogens. *Science* **324**, 742 (2009). doi:10.1126/science.1171647 Medline

3. P. N. Dodds, J. P. Rathjen, Plant immunity: Towards an integrated view of plant-pathogen interactions. *Nat. Rev. Genet.* **11**, 539 (2010). doi:10.1038/nrg2812 Medline

4. J. L. Dangl, J. D. Jones, Plant pathogens and integrated defence responses to infection. *Nature* **411**, 826 (2001). doi:10.1038/35081161 Medline

5. J. D. Jones, J. L. Dangl, The plant immune system. *Nature* **444**, 323 (2006). doi:10.1038/nature05286 Medline

6. E. Lukasik, F. L. Takken, STANDing strong, resistance proteins instigators of plant defence. *Curr. Opin. Plant Biol.* **12**, 427 (2009). doi:10.1016/j.pbi.2009.03.001 Medline

7. G. van Ooijen *et al*., Structure-function analysis of the NB-ARC domain of plant disease resistance proteins. *J. Exp. Bot.* **59**, 1383 (2008). doi:10.1093/jxb/ern045 Medline

8. D. A. Baltrus *et al*., Dynamic evolution of pathogenicity revealed by sequencing and comparative genomics of 19 *Pseudomonas syringae* isolates. *PLoS Pathog.* **7**, e1002132 (2011). doi:10.1371/journal.ppat.1002132

9. L. Baxter *et al*., Signatures of adaptation to obligate biotrophy in the *Hyaloperonospora arabidopsidis* genome. *Science* **330**, 1549 (2010). doi:10.1126/science.1195203 Medline

10. Glossary, materials and methods, supporting figures, and supporting tables are available as supporting material on *Science* Online.

11. *Arabidopsis* Interactome Mapping Consortium. *Science* **333**, 601 (2010).

12. M. Dreze *et al*., High-quality binary interactome mapping. *Methods Enzymol.* **470**, 281 (2010). doi:10.1016/S0076-6879(10)70012-4 Medline

13. P. Braun *et al*., An experimentally derived confidence score for binary protein-protein interactions. *Nat. Methods* **6**, 91 (2009). doi:10.1038/nmeth.1281 Medline

14. M. E. Cusick *et al*., Literature-curated protein interaction datasets. *Nat. Methods* **6**, 39 (2009). doi:10.1038/nmeth.1284 Medline

15. H. Yu *et al*., High-quality binary protein interaction map of the yeast interactome network. *Science* **322**, 104 (2008). doi:10.1126/science.1158684 Medline

16. J. D. Lewis, D. S. Guttman, D. Desveaux, The targeting of plant cellular systems by injected type III effector proteins. *Semin. Cell Dev. Biol.* **20**, 1055 (2009). doi:10.1016/j.semcdb.2009.06.003 Medline

17. Z. Y. Peng *et al*., *Arabidopsis* Hormone Database: A comprehensive genetic and phenotypic information database for plant hormone research in *Arabidopsis*. *Nucleic Acids Res.* **37**, (Database issue), D975 (2009). doi:10.1093/nar/gkn873 Medline

18. X. Tan *et al*., Global expression analysis of nucleotide binding site-leucine rich repeat-encoding and related genes in *Arabidopsis*. *BMC Plant Biol.* **7**, 56 (2007). doi:10.1186/1471-2229-7-56 Medline

19. C. Zipfel *et al*., Bacterial disease resistance in *Arabidopsis* through flagellin perception. *Nature* **428**, 764 (2004). doi:10.1038/nature02485 Medline

20. T. B. Sackton *et al*., Dynamic evolution of the innate immune system in *Drosophila*. *Nat. Genet.* **39**, 1461 (2007). doi:10.1038/ng.2007.60 Medline

21. E. B. Holub, The arms race is ancient history in *Arabidopsis*, the wildflower. *Nat. Rev. Genet.* **2**, 516 (2001). doi:10.1038/35080508 Medline

22. P. Zhang *et al*., MetaCyc and AraCyc. Metabolic pathway databases for plant research. *Plant Physiol.* **138**, 27 (2005). doi:10.1104/pp.105.060376 Medline

23. Y. Jaillais, J. Chory, Unraveling the paradoxes of plant hormone signaling integration. *Nat. Struct. Mol. Biol.* **17**, 642 (2010). doi:10.1038/nsmb0610-642 Medline

24. R. Albert, H. Jeong, A. L. Barabasi, Error and attack tolerance of complex networks. *Nature* **406**, 378 (2000). doi:10.1038/35019019 Medline

25. B. de Chassey *et al*., Hepatitis C virus infection protein network. *Mol. Syst. Biol.* **4**, 230 (2008). doi:10.1038/msb.2008.66 Medline

26. M. D. Dyer *et al*., The human-bacterial pathogen protein interaction networks of *Bacillus anthracis*, *Francisella tularensis*, and *Yersinia pestis*. *PLoS ONE* **5**, e12089 (2010). doi:10.1371/journal.pone.0012089 Medline

27. M. A. Calderwood *et al*., Epstein-Barr virus and virus human protein interaction maps. *Proc. Natl. Acad. Sci. U.S.A.* **104**, 7606 (2007). doi:10.1073/pnas.0702332104 Medline

28. P. Uetz *et al*., Herpesviral protein networks and their interaction with the human proteome. *Science* **311**, 239 (2006). doi:10.1126/science.1116804 Medline

29. J. M. Alonso *et al*., Genome-wide insertional mutagenesis of *Arabidopsis thaliana*. *Science* **301**, 653 (2003). doi:10.1126/science.1086391 Medline

30. A. Sessions *et al*., A high-throughput *Arabidopsis* reverse genetics system. *Plant Cell* **14**, 2985 (2002). doi:10.1105/tpc.004630 Medline

31. R. Lozano-Durán *et al*., Geminiviruses subvert ubiquitination by altering CSN-mediated derubylation of SCF E3 ligase complexes and inhibit jasmonate signaling in *Arabidopsis thaliana*. *Plant Cell* **23**, 1014 (2011). doi:10.1105/tpc.110.080267 Medline

32. G. Gusmaroli, P. Figueroa, G. Serino, X. W. Deng, Role of the MPN subunits in COP9 signalosome assembly and activity, and their regulatory interaction with *Arabidopsis* Cullin3-based E3 ligases. *Plant Cell* **19**, 564 (2007). doi:10.1105/tpc.106.047571 Medline

33. S. Robatzek, D. Chinchilla, T. Boller, Ligand-induced endocytosis of the pattern recognition receptor FLS2 in *Arabidopsis*. *Genes Dev.* **20**, 537 (2006). doi:10.1101/gad.366506 Medline

34. K. Tsuda, M. Sato, J. Glazebrook, J. D. Cohen, F. Katagiri, Interplay between MAMP-triggered and SA-mediated defense responses. *Plant J.* **53**, 763 (2008). doi:10.1111/j.1365-313X.2007.03369.x Medline

35. Acknowledgments (see text).

36. S. H. Shiu, A. B. Bleecker, Plant receptor-like kinase gene family: Diversity, function, and signaling. *Sci. STKE* **2001**, re22 (2001).doi:10.1126/stke.2001.113.re22 Medline

37. C. Zipfel *et al*., Perception of the bacterial PAMP EF-Tu by the receptor EFR restricts *Agrobacterium*-mediated transformation. *Cell* **125**, 749 (2006).doi:10.1016/j.cell.2006.03.037 Medline

38. C. Zipfel, J. P. Rathjen, Plant immunity: AvrPto targets the frontline. *Curr. Biol.* **18**, R218 (2008).doi:10.1016/j.cub.2008.01.016 Medline

39. L. Navarro *et al*., The transcriptional innate immune response to flg22. Interplay and overlap with Avr gene-dependent defense responses and bacterial pathogenesis. *Plant Physiol.* **135**, 1113 (2004).doi:10.1104/pp.103.036749 Medline

40. T. K. Eitas, J. L. Dangl, NB-LRR proteins: Pairs, pieces, perception, partners, and pathways. *Curr. Opin. Plant Biol.* **13**, 472 (2010).doi:10.1016/j.pbi.2010.04.007 Medline

41. J. W. Mansfield, From bacterial avirulence genes to effector functions via the *hrp* delivery system: an overview of 25 years of progress in our understanding of plant innate immunity. *Mol. Plant Pathol.* **10**, 721 (2009).doi:10.1111/j.1364-3703.2009.00576.x Medline

42. J. Win *et al*., Adaptive evolution has targeted the C-terminal domain of the RXLR effectors of plant pathogenic oomycetes. *Plant Cell* **19**, 2349 (2007).doi:10.1105/tpc.107.051037 Medline

43. M. Boxem *et al*., A protein domain-based interactome network for *C. elegans* early embryogenesis. *Cell* **134**, 534 (2008).doi:10.1016/j.cell.2008.07.009 Medline

44. N. Simonis *et al*., Empirically controlled mapping of the *Caenorhabditis elegans* protein-protein interactome network. *Nat. Methods* **6**, 47 (2009).doi:10.1038/nmeth.1279 Medline

45. K. Venkatesan *et al*., An empirical framework for binary interactome mapping. *Nat. Methods* **6**, 83 (2009).doi:10.1038/nmeth.1280 Medline

46. M. Ashburner *et al*.; The Gene Ontology Consortium, Gene ontology: Tool for the unification of biology. *Nat. Genet.* **25**, 25 (2000).doi:10.1038/75556 Medline

47. G. F. Berriz, J. E. Beaver, C. Cenik, M. Tasan, F. P. Roth, Next generation software for functional trend analysis. *Bioinformatics* **25**, 3043 (2009).doi:10.1093/bioinformatics/btp498 Medline

48. A. C. Berglund, E. Sjölund, G. Ostlund, E. L. Sonnhammer, InParanoid 6: Eukaryotic ortholog clusters with inparalogs. *Nucleic Acids Res.* **36**, (Database issue), D263 (2008).doi:10.1093/nar/gkm1020 Medline

49. D. Chandran, N. Inada, G. Hather, C. K. Kleindt, M. C. Wildermuth, Laser microdissection of *Arabidopsis* cells at the powdery mildew infection site reveals site-specific processes

and regulators. *Proc. Natl. Acad. Sci. U.S.A.* **107**, 460 (2010).doi:10.1073/pnas.0912492107 Medline

50. M. de Torres-Zabala *et al*., *Pseudomonas syringae* pv. *tomato* hijacks the *Arabidopsis* abscisic acid signalling pathway to cause disease. *EMBO J.* **26**, 1434 (2007).doi:10.1038/sj.emboj.7601575 Medline

51. C. Denoux *et al*., Activation of defense response pathways by OGs and Flg22 elicitors in *Arabidopsis* seedlings. *Mol. Plant* **1**, 423 (2008).doi:10.1093/mp/ssn019 Medline

52. T. Eulgem *et al*., Gene expression signatures from three genetically separable resistance gene signaling pathways for downy mildew resistance. *Plant Physiol.* **135**, 1129 (2004).doi:10.1104/pp.104.040444 Medline

53. H. Goda *et al*., The AtGenExpress hormone and chemical treatment data set: Experimental design, data evaluation, model data analysis and data access. *Plant J.* **55**, 526 (2008).doi:10.1111/j.1365-313X.2008.03510.x Medline

54. K. Ramonell *et al*., Loss-of-function mutations in chitin responsive genes show increased susceptibility to the powdery mildew pathogen *Erysiphe cichoracearum*. *Plant Physiol.* **138**, 1027 (2005).doi:10.1104/pp.105.060947 Medline

55. R. Thilmony, W. Underwood, S. Y. He, Genome-wide transcriptional analysis of the *Arabidopsis thaliana* interaction with the plant pathogen *Pseudomonas syringae* pv. *tomato* DC3000 and the human pathogen *Escherichia coli* O157:H7. *Plant J.* **46**, 34 (2006).doi:10.1111/j.1365-313X.2006.02725.x Medline

56. D. Wang, N. Amornsiripanitch, X. Dong, A genomic approach to identify regulatory nodes in the transcriptional network of systemic acquired resistance in plants. *PLoS Pathog.* **2**, e123 (2006).doi:10.1371/journal.ppat.0020123 Medline

57. S. F. Altschul, W. Gish, W. Miller, E. W. Myers, D. J. Lipman, Basic local alignment search tool. *J. Mol. Biol.* **215**, 403 (1990). Medline

58. M. A. Larkin *et al*., Clustal W and Clustal X version 2.0. *Bioinformatics* **23**, 2947 (2007).doi:10.1093/bioinformatics/btm404 Medline

59. Z. Yang, R. Nielsen, Estimating synonymous and nonsynonymous substitution rates under realistic evolutionary models. *Mol. Biol. Evol.* **17**, 32 (2000). Medline

60. Z. Yang, PAML 4: Phylogenetic analysis by maximum likelihood. *Mol. Biol. Evol.* **24**, 1586 (2007).doi:10.1093/molbev/msm088 Medline

61. G. Csárdi, T. Nepusz, The igraph library for complex network research. *Int. J. Complex Systems* **1695** (2006); http://igraf.sf.net.

62. P. Shannon *et al*., Cytoscape: A software environment for integrated models of biomolecular interaction networks. *Genome Res.* **13**, 2498 (2003).doi:10.1101/gr.1239303 Medline

63. M. G. Rosso *et al*., An *Arabidopsis thaliana* T-DNA mutagenized population (GABI-Kat) for flanking sequence tag-based reverse genetics. *Plant Mol. Biol.* **53**, 247 (2003).doi:10.1023/B:PLAN.0000009297.37235.4a Medline

64. K. Tatematsu, K. Nakabayashi, Y. Kamiya, E. Nambara, Transcription factor AtTCP14 regulates embryonic growth potential during seed germination in *Arabidopsis thaliana*. *Plant J.* **53**, 42 (2008).doi:10.1111/j.1365-313X.2007.03308.x Medline

65. G. Gusmaroli, S. Feng, X. W. Deng, The *Arabidopsis* CSN5A and CSN5B subunits are present in distinct COP9 signalosome complexes, and mutations in their JAMM domains exhibit differential dominant negative effects on development. *Plant Cell* **16**, 2984 (2004).doi:10.1105/tpc.104.025999 Medline

66. Y. Gu *et al*., Prefoldin 6 is required for normal microtubule dynamics and organization in *Arabidopsis*. *Proc. Natl. Acad. Sci. U.S.A.* **105**, 18064 (2008).doi:10.1073/pnas.0808652105 Medline

67. J. L. Dangl *et al*., in *Methods in* Arabidopsis *Research*, N. H. Chua, C. Koncz, and J. Schell, Eds. (World Scientific Publishing Co., London, 1992), pp. 393–418.

68. E. B. Holub, J. L. Beynon, Symbiology of mouse-ear cress (*Arabidopsis thaliana*) and oomycetes. *Adv. Bot. Res.* **24**, 227 (1997). doi:10.1016/S0065-2296(08)60075-0

69. E. Koch, A. Slusarenko, *Arabidopsis* is susceptible to infection by a downy mildew fungus. *Plant Cell* **2**, 437 (1990). Medline

70. B. F. Holt, 3rd, Y. Belkhadir, J. L. Dangl, Antagonistic control of disease resistance protein stability in the plant immune system. *Science* **309**, 929 (2005).doi:10.1126/science.1109977 Medline

71. P. C. Stirling, S. F. Bakhoum, A. B. Feigl, M. R. Leroux, Convergent evolution of clamp-like binding sites in diverse chaperones. *Nat. Struct. Mol. Biol.* **13**, 865 (2006).doi:10.1038/nsmb1153 Medline

72. A. V. García, J. E. Parker, Heaven's Gate: Nuclear accessibility and activities of plant immune regulators. *Trends Plant Sci.* **14**, 479 (2009).doi:10.1016/j.tplants.2009.07.004 Medline

73. T. K. Eitas, Z. L. Nimchuk, J. L. Dangl, *Arabidopsis* TAO1 is a TIR-NB-LRR protein that contributes to disease resistance induced by the *Pseudomonas syringae* effector AvrB. *Proc. Natl. Acad. Sci. U.S.A.* **105**, 6475 (2008).doi:10.1073/pnas.0802157105 Medline

74. M. Martín-Trillo, P. Cubas, TCP genes: A family snapshot ten years later. *Trends Plant Sci.* **15**, 31 (2010).doi:10.1016/j.tplants.2009.11.003 Medline

75. P. J. Rushton, I. E. Somssich, P. Ringler, Q. J. Shen, WRKY transcription factors. *Trends Plant Sci.* **15**, 247 (2010).doi:10.1016/j.tplants.2010.02.006 Medline

76. T. V. Huynh, D. Dahlbeck, B. J. Staskawicz, Bacterial blight of soybean: Regulation of a pathogen gene determining host cultivar specificity. *Science* **245**, 1374 (1989).doi:10.1126/science.2781284 Medline

77. L. Du *et al*., Ca(2+)/calmodulin regulates salicylic-acid-mediated plant immunity. *Nature* **457**, 1154 (2009).doi:10.1038/nature07612 Medline

78. L. E. Sander *et al*., Detection of prokaryotic mRNA signifies microbial viability and promotes immunity. *Nature* **474**, 385 (2011).doi:10.1038/nature10072 Medline

79. D. A. Chamovitz, Revisiting the COP9 signalosome as a transcriptional regulator. *EMBO Rep.* **10**, 352 (2009).doi:10.1038/embor.2009.33 Medline

80. A. Capron *et al*., The *Arabidopsis* anaphase-promoting complex or cyclosome: Molecular and genetic characterization of the APC2 subunit. *Plant Cell* **15**, 2370 (2003).doi:10.1105/tpc.013847 Medline

81. L. J. Kong, L. Hanley-Bowdoin, A geminivirus replication protein interacts with a protein kinase and a motor protein that display different expression patterns during plant development and infection. *Plant Cell* **14**, 1817 (2002).doi:10.1105/tpc.003681 Medline

82. J. Y. Xiong *et al*., Recruitment of AtWHY1 and AtWHY3 by a distal element upstream of the kinesin gene AtKP1 to mediate transcriptional repression. *Plant Mol. Biol.* **71**, 437 (2009).doi:10.1007/s11103-009-9533-7 Medline

83. D. Swarbreck *et al*., The *Arabidopsis* Information Resource (TAIR): Gene structure and function annotation. *Nucleic Acids Res.* **36**, (Database issue), D1009 (2008).doi:10.1093/nar/gkm965 Medline

84. B. Aranda *et al*., The IntAct molecular interaction database in 2010. *Nucleic Acids Res.* **38**, (Database issue), D525 (2010).doi:10.1093/nar/gkp878 Medline

85. C. Stark *et al*., BioGRID: A general repository for interaction datasets. *Nucleic Acids Res.* **34**, (Database issue), D535 (2006).doi:10.1093/nar/gkj109 Medline

86. P. Li *et al*., Fructose sensitivity is suppressed in *Arabidopsis* by the transcription factor ANAC089 lacking the membrane-bound domain. *Proc. Natl. Acad. Sci. U.S.A.* **108**, 3436 (2011).doi:10.1073/pnas.1018665108 Medline

87. J. Li, J. Zhang, X. Wang, J. Chen, A membrane-tethered transcription factor ANAC089 negatively regulates floral initiation in *Arabidopsis thaliana*. *Sci. China Life Sci.* **53**, 1299 (2010).doi:10.1007/s11427-010-4085-2 Medline

88. P. Zimmermann, M. Hirsch-Hoffmann, L. Hennig, W. Gruissem, GENEVESTIGATOR. *Arabidopsis* microarray database and analysis toolbox. *Plant Physiol.* **136**, 2621 (2004).doi:10.1104/pp.104.046367 Medline

89. T. Kamiya *et al*., NIP1;1, an aquaporin homolog, determines the arsenite sensitivity of *Arabidopsis thaliana*. *J. Biol. Chem.* **284**, 2114 (2009).doi:10.1074/jbc.M806881200 Medline

90. T. Kamiya, T. Fujiwara, *Arabidopsis* NIP1;1 transports antimonite and determines antimonite sensitivity. *Plant Cell Physiol.* **50**, 1977 (2009).doi:10.1093/pcp/pcp130 Medline

91. B. A. Adie *et al*., ABA is an essential signal for plant resistance to pathogens affecting JA biosynthesis and the activation of defenses in *Arabidopsis*. *Plant Cell* **19**, 1665 (2007).doi:10.1105/tpc.106.048041 Medline

92. H. K. Yoon, S. G. Kim, S. Y. Kim, C. M. Park, Regulation of leaf senescence by NTL9-mediated osmotic stress signaling in *Arabidopsis*. *Mol. Cells* **25**, 438 (2008). Medline

93. V. A. Voelz, G. R. Bowman, K. Beauchamp, V. S. Pande, Molecular simulation of ab initio protein folding for a millisecond folder NTL9(1-39). *J. Am. Chem. Soc.* **132**, 1526 (2010).doi:10.1021/ja9090353 Medline

94. M. S. Mukhtar, M. T. Nishimura, J. Dangl, NPR1 in plant defense: It's not over 'til it's turned over. *Cell* **137**, 804 (2009).doi:10.1016/j.cell.2009.05.010 Medline

95. S. R. Hind *et al*., The COP9 signalosome controls jasmonic acid synthesis and plant responses to herbivory and pathogens. *Plant J.* **65**, 480 (2011).doi:10.1111/j.1365-313X.2010.04437.x Medline

96. K. Tatematsu, K. Nakabayashi, Y. Kamiya, E. Nambara, Transcription factor AtTCP14 regulates embryonic growth potential during seed germination in *Arabidopsis thaliana*. *Plant J.* **53**, 42 (2008).doi:10.1111/j.1365-313X.2007.03308.x Medline

97. L. Navarro *et al*., DELLAs control plant immune responses by modulating the balance of jasmonic acid and salicylic acid signaling. *Curr. Biol.* **18**, 650 (2008).doi:10.1016/j.cub.2008.03.060 Medline

98. N. H. Petersen *et al*., Identification of proteins interacting with *Arabidopsis* ACD11. *J. Plant Physiol.* **166**, 661 (2009).doi:10.1016/j.jplph.2008.08.003 Medline

99. J. E. Carette *et al*., Characterization of plant proteins that interact with cowpea mosaic virus '60K' protein in the yeast two-hybrid system. *J. Gen. Virol.* **83**, 885 (2002). Medline

100. F. Laurent, G. Labesse, P. de Wit, Molecular cloning and partial characterization of a plant VAP33 homologue with a major sperm protein domain. *Biochem. Biophys. Res. Commun.* **270**, 286 (2000).doi:10.1006/bbrc.2000.2387 Medline

101. M. Lewandowska *et al*., A contribution to identification of novel regulators of plant response to sulfur deficiency: Characteristics of a tobacco gene UP9C, its protein product and the effects of UP9C silencing. *Mol. Plant* **3**, 347 (2010).doi:10.1093/mp/ssq007 Medline

102. K. Baba, T. Nakano, K. Yamagishi, S. Yoshida, Involvement of a nuclear-encoded basic helix-loop-helix protein in transcription of the light-responsive promoter of psbD. *Plant Physiol.* **125**, 595 (2001).doi:10.1104/pp.125.2.595 Medline

103. I. Efroni, E. Blum, A. Goldshmidt, Y. Eshed, A protracted and dynamic maturation schedule underlies *Arabidopsis* leaf development. *Plant Cell* **20**, 2293 (2008).doi:10.1105/tpc.107.057521 Medline

104. D. Garbe, J. B. Doto, M. V. Sundaram, *Caenorhabditis elegans* lin-35/Rb, efl-1/E2F and other synthetic multivulva genes negatively regulate the anaphase-promoting complex gene mat-3/APC8. *Genetics* **167**, 663 (2004).doi:10.1534/genetics.103.026021 Medline

105. B. Zheng, X. Chen, S. McCormick, The anaphase-promoting complex is a dual integrator that regulates both MicroRNA-mediated transcriptional regulation of cyclin B1 and degradation of Cyclin B1 during *Arabidopsis* male gametophyte development. *Plant Cell* **23**, 1033 (2011).doi:10.1105/tpc.111.083980 Medline

106. I. L. Viola, N. G. Uberti Manassero, R. Ripoll, D. H. Gonzalez, The *Arabidopsis* class I TCP transcription factor AtTCP11 is a developmental regulator with distinct DNA-binding properties due to the presence of a threonine residue at position 15 of the TCP domain. *Biochem. J.* **435**, 143 (2011).doi:10.1042/BJ20101019 Medline

107. X. Y. Yang *et al*., *Arabidopsis* kinesin KP1 specifically interacts with VDAC3, a mitochondrial protein, and regulates respiration during seed germination at low temperature. *Plant Cell* **23**, 1093 (2011).doi:10.1105/tpc.110.082420 Medline

108. S. Saiga *et al*., The *Arabidopsis* OBERON1 and OBERON2 genes encode plant homeodomain finger proteins and are required for apical meristem maintenance. *Development* **135**, 1751 (2008).doi:10.1242/dev.014993 Medline

109. G. C. Pagnussat *et al*., Genetic and molecular identification of genes required for female gametophyte development and function in *Arabidopsis*. *Development* **132**, 603 (2005).doi:10.1242/dev.01595 Medline

110. A. Chini *et al*., The JAZ family of repressors is the missing link in jasmonate signalling. *Nature* **448**, 666 (2007).doi:10.1038/nature06006 Medline

111. L. Hughes-Davies *et al*., EMSY links the BRCA2 pathway to sporadic breast and ovarian cancer. *Cell* **115**, 523 (2003).doi:10.1016/S0092-8674(03)00930-9 Medline

112. S. Wang, W. E. Durrant, J. Song, N. W. Spivey, X. Dong, *Arabidopsis* BRCA2 and RAD51 proteins are specifically involved in defense gene transcription during plant immune responses. *Proc. Natl. Acad. Sci. U.S.A.* **107**, 22716 (2010).doi:10.1073/pnas.1005978107 Medline

113. N. Frey dit Frey *et al.*, The RNA binding protein Tudor-SN is essential for stress tolerance and stabilizes levels of stress-responsive mRNAs encoding secreted proteins in *Arabidopsis. Plant Cell* **22**, 1575 (2010).

114. S. Liu, J. Jia, Y. Gao, B. Zhang, Y. Han, The AtTudor2, a protein with SN-Tudor domains, is involved in control of seed germination in *Arabidopsis*. *Planta* **232**, 197 (2010).doi:10.1007/s00425-010-1167-0 Medline